Check for updates

Earthquake Spectra

RESEARCH PAPER

Effective Seismic Retrofit of URM Parapets Using Mechanical Anchors as Vertical Reinforcement

Jerry Y. Zhai[1] | Francisco Galvez[2] | Eyitayo A. Opabola[1] | Dmytro Dizhur[3] | Robert Hudson[4] | David Sommer[5]

[1]Department of Civil Engineering, University of California, Berkeley, California, USA | [2]Python Fixings, Auckland, New Zealand | [3]Dizhur Consulting, Auckland, New Zealand | [4]Python Fasteners U.S., Seattle, Washington, USA | [5]Degenkolb Engineers, Seattle, Washington, USA

Correspondence: Jerry Y. Zhai (jerryzhai@berkeley.edu)

Received: 30 April 2025 | **Revised:** 12 January 2026 | **Accepted:** 26 February 2026

Keywords: anchor reinforcement | ASCE 41 | design equations | masonry anchor | parapet strengthening | seismic strengthening | unreinforced masonry retrofit | URM

ABSTRACT

The development of cost-effective and minimally invasive retrofit strategies to address the seismic vulnerabilities of unreinforced brick masonry (URM) parapets in heritage buildings is crucial to both community resilience and preservation of cultural landmarks. This study presents an experimental program investigating the out-of-plane lateral response of 11 full-scale URM parapet specimens, retrofitted using postinstalled small-diameter mechanical anchors as vertical reinforcement. Test variables include loading protocol (i.e., cyclic vs. monotonic), anchorage configuration, anchorage embedment, and presence of strongbacks. The experimental results show that the lateral strength of the retrofitted specimens ranges from about 5 to 25 times greater than the postcracked rocking strength of the as-built specimens. Leveraging the experimental results and the identified impact of the test variables on retrofit effectiveness, using a strength hierarchy approach, this study proposes semiempirical nominal strength equations and capacity reduction factors that can be adopted by engineers to design retrofit strategies for URM parapets using mechanical anchors. Validation using the test data shows a R^2 value of 0.75 and a failure mode prediction accuracy of 84%.

1 | Introduction

Traditional masonry construction in heritage buildings often lacks proper reinforcement, making these structures susceptible to catastrophic failures during seismic events. The significant damages to about 200 school buildings constructed with unreinforced masonry (URM) facades following the 1933 Long Beach earthquake in California highlighted the severe seismic risk of URM structures (NGDC 2009). A ban on URM construction soon followed. Subsequent major earthquakes (e.g., the 1971 San Fernando and the 1989 Loma Prieta earthquakes) further highlighted the vulnerabilities of URM structures. Typical observed failure mechanisms include the out-of-plane collapse of walls, in-plane shear failure, and partial or complete separation of walls and floors or roofs (Dizhur et al. 2011). These vulnerabilities highlighted the critical need for retrofitting existing URM buildings to protect against collapse, which resulted in ordinances requiring seismic retrofits for URM structures (California Seismic Safety Commission 1992).

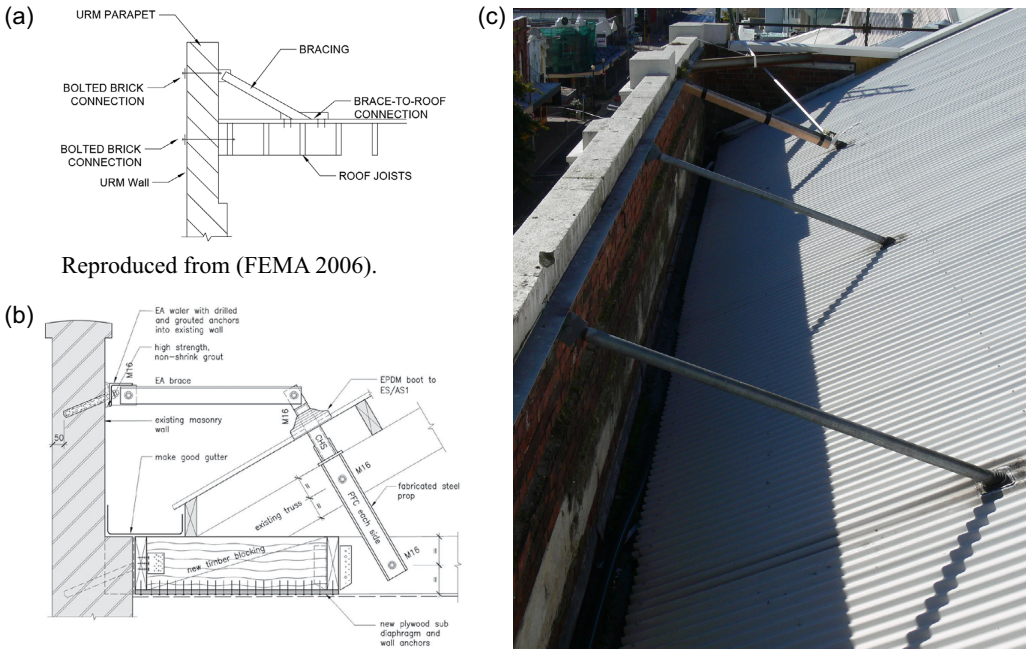
URM parapets are particularly vulnerable during seismic events due to their lack of lateral support, weathering on both faces of the parapet, and exposure to significant accelerations (FEMA 2012) and have a well-documented history of

© 2026 Earthquake Engineering Research Institute.

collapse in multiple major earthquakes, including the 1989 Loma Prieta, the 1994 Northridge, and the 2011 Christchurch earthquakes (Bruneau 1995; Giaretton et al. 2016; NGDC 2009). Inventory studies of URM parapets globally have highlighted the dangers of parapet collapse to pedestrians, occupants, and adjacent structures. For example, approximately 60% of the nearly 600 URM parapets in the Christchurch, New Zealand, area are street facing and located on two-story buildings, presenting a significant hazard to the street level (Giaretton et al. 2016). The fragility data developed in FEMA P-58 (FEMA 2018) for URM parapets also highlight that parapet failure result in losses and recovery downtime after earthquakes. Hence, in addition to retrofitting primary structural elements, addressing URM parapets is a critical aspect of seismic risk mitigation.

The current industry practice for parapet retrofit is to use steel or timber braces/backstays to provide lateral support and enhance the in-plane and out-of-plane capacity of URM parapets (Cassol et al. 2025; FEMA 2006; Giaretton et al. 2017) (see Figure 1). Studies of this retrofit practice (e.g., Dizhur et al. 2017; Sommer et al. 2019) and field observations following earthquakes (FEMA 2015) have demonstrated that earthquake safety is sufficiently provided. Other studies (e.g., Elgawady 2004; Mercimek et al. 2025) have demonstrated the effectiveness of fiber-reinforced polymer (FRP) strips or sheets in strengthening URM parapets and improving their resistance to both in-plane and out-of-plane forces. Similarly, reinforced cores are a well-established technique for strengthening URM walls for both in-plane and out-of-plane actions (Farahani et al. 2021; FEMA 2006; New Zealand Ministry of Business 2018) commonly used in historically or architecturally sensitive buildings because the core is internal and exterior/interior faces require limited finishing. Furthermore, studies (Borri et al. 2011; Yılmaz et al. 2024) have explored seismic retrofit (in-plane and out-of-plane) of URM walls using different innovative materials (e.g., cementitious matrix grid) for surface treatment.

While the retrofit techniques discussed above are effective, a few challenges affect their practicality. For example, seismic retrofit of URM parapets using backstays can be invasive, often requiring significant structural alterations that may compromise the architectural integrity of heritage buildings. For parapets, the backstays must be anchored at some location at the roof level, compromising the waterproofing membrane. Also, backstays can impede usable roof space for URM buildings where the roof is in service because backstays must not be constructed with a steep bracing angle. Studies have shown that backstays with steep bracing angles can result in premature failure due to the uplift forces exerted onto the masonry during reversal of applied loadings (Giaretton et al. 2018). Depending on various factors, this retrofit technique may be too expensive and not feasible for structures with limited budgets. Regarding reinforced cores, the main drawback of the system is the need to drill a large-diameter hole to insert the steel reinforcement and grout. Traditionally, coring relied on water-cooled diamond bits, which generated slurry that could stain and damage sensitive heritage



Reproduced from (FEMA 2006).

Reproduced from (New Zealand Ministry of Business, 2018)

Real example (Giaretton et al., 2016).

FIGURE 1 | Parapet wall specimens with backstay system anchored to roof. (a) Reproduced from FEMA (2006). (b) Reproduced from New Zealand Ministry of Business (2018). (c) Real example (Giaretton et al. 2016).

19448201, 2026, 2, Downloaded from https://onlinelibrary.wiley.com/doi/10.1002/eqs4.70065 by University Of Auckland, Wiley Online Library on [24/06/2026]. See the Terms and Conditions (https://onlinelibrary.wiley.com/terms-and-conditions) on Wiley Online Library for rules of use; OA articles are governed by the applicable Creative Commons License

surfaces. More recent practice has shifted to dry drilling equipment operating at low rotational speeds, allowing the core material to be removed in solid pieces. However, the combination of slow drilling, large hole diameters, and the subsequent placement of grout and reinforcement can make this technique costly. As for FRP retrofit methods, concerns such as cost, installation on both parapet faces resulting in alterations to the facade, and sensitivity to environmental factors such as high temperatures and humidity may decrease the FRP method's desirability. Similarly, the weight added by surface treatment techniques (e.g., shotcrete) can undesirably increase seismic demands on structural components and are difficult to reverse.

As demonstrated by Tong et al. (2022) in a comparative study of seismic retrofit programs in the United States and New Zealand, successful seismic retrofits of URM buildings strongly depend on a combination of financial, technical, and administrative measures. Offering alternative, innovative, and economical retrofit design solutions is a key contributor to the success of heritage building strengthening, where traditional methods may be invasive or prohibitively expensive, and can make the difference between a successful retrofit and a project that results in demolition.

In this context, postinstalled small-diameter mechanical anchors are a more cost-effective and less invasive solution for retrofitting URM parapets to improve their seismic performance than the reviewed techniques. These anchors are used to secure parapets to the main structural system, such as the roof diaphragms or adjacent walls, providing additional lateral stability and reducing the risk of out-of-plane collapse during seismic events. To avoid the disadvantages of the aforementioned techniques for URM parapet retrofit, this article describes a cost-effective technique with minimal architectural alteration, using mechanical anchors that secure URM parapets to the roof diaphragm. The anchors are embedded to a nominal distance below the roof diaphragm such that the parapet is secured against seismic failure. By introducing steel anchors to the masonry wall that will contribute to out-of-plane actions, design approaches related to reinforced masonry parapets can be adapted for use in these retrofitted parapets (Paulay and Priestly 1992).

A series of experimental tests on 11 representative parapet specimens were conducted, yielding 25 unique data points for URM parapet walls retrofitted with postinstalled mechanical anchors. The parapet specimens were constructed with heritage brick and heritage mortar to represent the traditional characteristics of URM construction in this region. The experimental data is presented and used to calibrate retrofit design equations that are compatible with ASCE/SEI 41-23 guidelines (ASCE 2023) for seismic retrofit. A discussion of the critical limit states for design are presented and discussed. While parapets are classified as acceleration sensitive nonstructural components and therefore designed for forces, the tests show that the retrofit with mechanical anchors can also undergo significant inelastic deformation during out-of-plane loading.

2 | Research Significance

Seismic retrofit of URM structures with minimally invasive, cost-effective methods is a critical gap in seismic risk mitigation for heritage buildings. This article proposes a solution of postinstalled small-diameter mechanical anchors as vertical reinforcement to reinforce URM parapets against out-of-plane collapse during earthquakes. The experimental program to validate this approach is described, and the retrofit effectiveness is quantified. Equations for retrofitted capacity are provided for design purposes.

3 | Experimental Program

Eleven parapet specimens in various geometric configurations were constructed with heritage brick and heritage mortar, with a typical specimen shown in Figure 2. The main test variables between the specimens are (a) parapet height, (b) diaphragm elevation, (c) the number and spacing of mechanical anchors, (d) the loading protocol, and (e) the presence/absence of vertical wooden members, termed strongbacks, fixed in the interior surface of the wall below roof diaphragm level as a strengthening solution. All parapet specimens were approximately 1000 mm (39″) wide and constructed as either one-wythe or two-wythe walls that were 115 mm (4.5″) or 230 mm (9″) thick. The parapet height ranges from 400 to 1010 mm (15.7″ to 39.8″) (i.e., the parapet height-to-thickness ratio ranges from 1.7 to 4.4, with varying diaphragm elevations depending on the total parapet height). The specimen dimensions were based on observations from Giaretton et al. (2016), which documented typical construction details of New Zealand URM buildings.

As summarized in Table 1, specimens were tested under either monotonic or cyclic quasistatic out-of-plane loading protocols to evaluate the impact of loading history on strength, deformation capacity, and damage accumulation. Additional discussions on the loading protocol are provided subsequently in this article. The spacing of vertical mechanical anchors

19448201, 2026, 2, Downloaded from https://onlinelibrary.wiley.com/doi/10.1002/eqs4.70065 by University Of Auckland, Wiley Online Library on [24/06/2026]. See the Terms and Conditions (https://onlinelibrary.wiley.com/terms-and-conditions) on Wiley Online Library for rules of use; OA articles are governed by the applicable Creative Commons License



FIGURE 2 | Typical test setup.

was varied to investigate the impact of anchor reinforcement ratio on the lateral strength of retrofitted parapet specimens (see Table 1). Four evenly spaced diaphragm anchors were used to connect the parapet specimen to the diaphragm.

In addition, selected specimens incorporated wooden strongbacks, which provide a tensile element to vertically spanning walls, which inherently lack tensile strength. This strengthening method has proven to be highly effective transferring out-of-plane wall loads to the diaphragms above and below. As a result, the strengthened wall exhibits greater out-of-plane moment capacity, enhancing its ability to withstand seismic accelerations (Dizhur et al. 2017; Cassol et al. 2021).

Axial loads due to self-weight and tributary roof loads were not included in the experimental setup or in the analytical formulation, as their contribution to anchor demand is on the order of 3%–4% of the forces at failure. Moreover, such axial loads would have a confining effect under the diaphragm and around the anchors; therefore, neglecting them was considered conservative for the purposes of this study.

In order to study the as-built capacity of the parapet, the initial horizontal crack was induced creating a weak plane of maximum bending moment at the diaphragm level by strengthening the masonry below the diaphragm with wooden strongbacks. Additionally, specimens cracked and retrofitted with mechanical anchors were tested with and without strongbacks to observe its effects on overall lateral strength, stiffness, and failure mechanism. The key details are summarized in Table 1, and the general specimen configuration is presented in Figure 3a.

Each test is identified by two naming formats: the Test ID format and the Parapet Name format. These separate formats help classify the parapet tests, as multiple tests were performed on a single parapet. The Test ID format is G*x*-*y*, where G*x* stands for the mortar group (see Table 1) and *y* represents a specific test number (e.g., G2–4 → Group 2 mortar, fourth test in this group). The Parapet Name format is #P*xn*-S*y*, where #P indicates a parapet, *x* indicates the mortar strength level (L = low, M = medium, and H = high), *n* corresponds to a physical parapet specimen, and S*y* corresponds to the sequence of tests performed on that specific parapet. Decimal values trailing *n* indicate a change in testing configuration using the same parapet.

4 | Material Properties

The mechanical anchors investigated in this experimental program are high-strength steel anchors ($\phi = 8$ mm [5/16″], $A_s = 50$ mm^2 [0.078 in^2]) with the base metal having a tensile strength of 57 kN (12.8 kip), corresponding to 1140 MPa (165 ksi). A spiral thread navigates the anchor circumference, providing a mechanical connection to the brick. The vertical anchors intended for parapet retrofit were prototyped by welding shorter anchor segments together to form a long, continuous anchor. Uniaxial testing of the vertical anchor prototypes showed a reduced capacity of 24 kN

19448201, 2026, 2, Downloaded from https://onlinelibrary.wiley.com/doi/10.1002/eqs4.70065 by University Of Auckland, Wiley Online Library on [24/06/2026]. See the Terms and Conditions (https://onlinelibrary.wiley.com/terms-and-conditions) on Wiley Online Library for rules of use; OA articles are governed by the applicable Creative Commons License

TABLE 1 | Overview of specimen geometry.

Test ID	Parapet name	Height (h)	Wythes	Num. anchors (N)	Anchor spacing (s_a)	Anchor embedment ($l_{emb,a}$)	Loading protocol	Strongbacks
G1-1	#PL1-S2	500 mm (19.7″)	2	2	480 mm (18.9″)	360 mm (14.2″)	Monotonic-push	No
G1-2	#PL1-S3	500 mm (19.7″)	2	2	480 mm (18.9″)	360 mm (14.2″)	Monotonic-push	Yes
G2-1	#PM1-S2	500 mm (19.7″)	1	2	480 mm (18.9″)	360 mm (14.2″)	Monotonic-push	No
G2-2	#PM1-S3	500 mm (19.7″)	1	2	480 mm (18.9″)	360 mm (14.2″)	Monotonic-push	Yes
G2-3	#PM2-S2	500 mm (19.7″)	2	2	480 mm (18.9″)	360 mm (14.2″)	Monotonic-push	No
G2-4	#PM2-S3	500 mm (19.7″)	2	2	480 mm (18.9″)	360 mm (14.2″)	Monotonic-push	Yes
G2-5	#PM3-S2	1010 mm (39.8″)	1	2	470 mm (18.5″)	25 mm (1″) (in concrete)	Monotonic-push	—
G2-6	#PM3-S3	1010 mm (39.8″)	1	2	470 mm (18.5″)	80 mm (3.2″) (in concrete)	Monotonic-push	—
G3-1	#PH1-S4	650 mm (25.6″)	2	2	500 mm (19.7″)	350 mm (13.8″)	Monotonic-push	Yes
G3-2	#PH2-S2	650 mm (25.6″)	2	3	250 mm (9.8″)	350 mm (13.8″)	Monotonic-push	Yes
G3-3	#PH2.1-S1	650 mm (25.6″)	2	1	—	350 mm (13.8″)	Cyclic	Yes
G3-4	#PH2.2-S2	400 mm (15.7″)	2	1	—	600 mm (23.6″)	Cyclic	Yes
G3-5	#PH3-S2	650 mm (25.6″)	2	2	500 mm (19.7″)	350 mm (13.8″)	Cyclic	Yes
G3-6	#PH3.1-S1	400 mm (15.7″)	2	2	500 mm (19.7″)	600 mm (23.6″)	Cyclic	Yes
G3-7a	#PH4-S2	650 mm (25.6″)	2	2	700 mm (27.6″)	350 mm (13.8″)	Cyclic	No
G3-7b	#PH4-S3	650 mm (25.6″)	2	2	700 mm (27.6″)	350 mm (13.8″)	Cyclic	Yes
G3-8	#PH4.1-S1	400 mm (15.7″)	2	2	700 mm (27.6″)	600 mm (23.6″)	Cyclic	Yes
G3-9a	#PH5-S2	900 mm (35.4″)	2	2	500 mm (19.7″)	300 mm (11.8″)	Cyclic	No
G3-9b	#PH5-S3	900 mm (35.4″)	2	2	500 mm (19.7″)	300 mm (11.8″)	Cyclic	Yes
G3-10	#PH5.1-S1	650 mm (25.6″)	2	2	500 mm (19.7″)	550 mm (21.7″)	Cyclic	Yes
G3-11a	#PH6-S2	400 mm (15.7″)	2	2	500 mm (19.7″)	600 mm (23.6″)	Cyclic	No
G3-11b	#PH6-S3	400 mm (15.7″)	2	2	500 mm (19.7″)	600 mm (23.6″)	Cyclic	Yes
G3-12	#PH7-S2	650 mm (25.6″)	2	1	—	80 mm (3.15″) (concrete)	Cyclic	—
G3-13	#PH7-S3	650 mm (25.6″)	2	2	500 mm (19.7″)	80 mm (3.15″) (concrete)	Cyclic	—

19448201, 2026, 2, Downloaded from https://onlinelibrary.wiley.com/doi/10.1002/eqsp4.70065 by University Of Auckland, Wiley Online Library on [24/06/2026]. See the Terms and Conditions (https://onlinelibrary.wiley.com/terms-and-conditions) on Wiley Online Library for rules of use; OA articles are governed by the applicable Creative Commons License

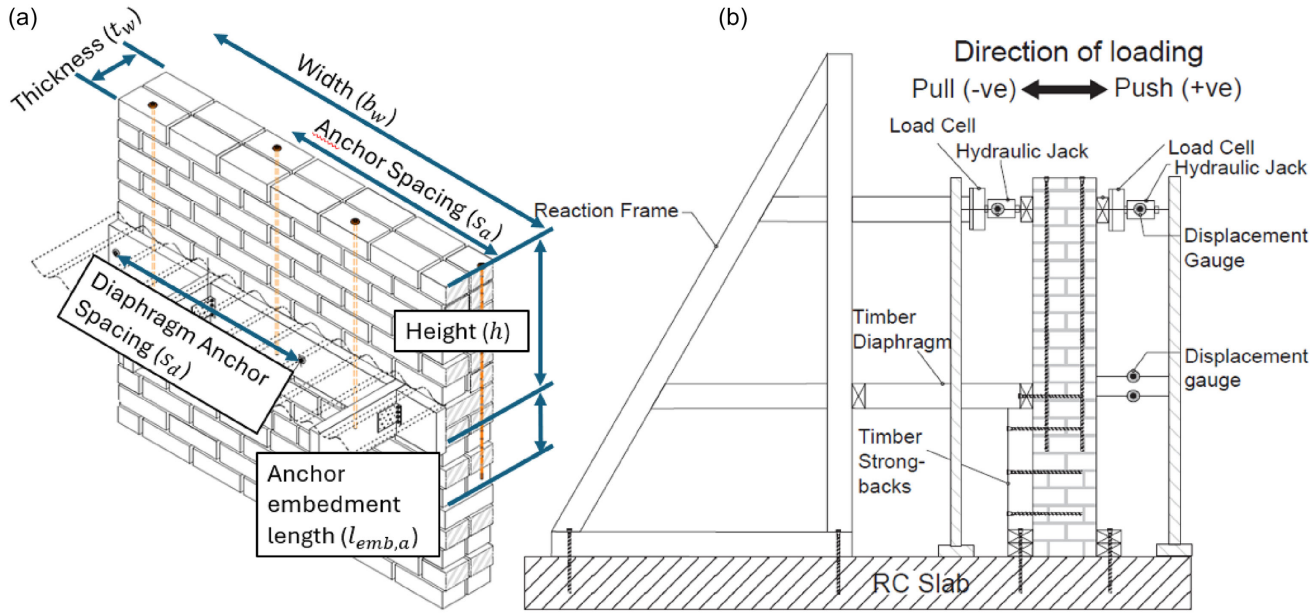


FIGURE 3 | (a) Specimen geometry and (b) testing configuration.

(5.4 kip) due to failure initiating at the welded segments. The prototype vertical anchors were either 860 mm (33.9 in), 1000 mm (39.4 in), or 1300 mm (51.2 in) long. The anchors and typical installation configuration are shown in Figure 4.

The heritage bricks used as part of this experimental program were reclaimed from vintage masonry buildings in New Zealand that were slated for demolition. These bricks had a mean compressive strength of 17.8 MPa (2.6 ksi) at a coefficient of variation (CoV) of 0.4, as determined through compressive testing of specimens sampled randomly, which showed individual strengths ranging from 6.6 to 29.5 MPa. This range falls within the classification for heritage bricks in New Zealand established by Lumantarna (2012) (8.5–43 MPa). The estimated tensile strength for the brick (f_t) and mortar (f_{tm}) was taken as 5% of the mean compressive strength for each material, respectively (f_c and f_{cm}) (Lourenco 1996). It was imperative to build specimens using heritage bricks to have a material representative of URM parapets requiring retrofit, with edges rounded due to long-term wear. Based on the mortar strength ranges proposed for heritage mortar in New Zealand (Lumantarna 2012), and guided by ASTM C1329-05 (ASTM 2005) and NZSEE (2017), compressive strengths ranging from 0.7 to 23 MPa are identified. For the purposes of this study, a more conservative range of 0.4–9.7 MPa was adopted, as summarized in Table 2.

Prior to designing the retrofit solution, a condition assessment of the brick and mortar should be carried out to identify degradation, loss of mortar depth, and local defects. Where necessary, repointing or local repair could be considered using compatible materials to improve the mechanical properties of the masonry before installing the mechanical anchors. This assessment is also important to establish an effective wall thickness for use in estimating the system capacity during design.

5 | Experimental Setup and Protocol

The parapet specimens were loaded quasistatically in the out-of-plane direction at the top of the wall specimen as depicted in Figure 3b. The applied load is restrained by a simulated diaphragm connection at the desired elevation and a support preventing lateral movement at the base of the parapet specimen. The diaphragm connection is secured to the parapet wall with timber planks and anchored with mechanical anchors passing through all brick wythes. This diaphragm connection provided an effective lateral restraint without restraining rotation. The base of the parapet wall was restrained against lateral movement by reacting against the 2×4 timber members that are anchored to the concrete slab. It was observed that the foot of the parapet wall was effectively restrained against lateral movement but allowed to rotate. Both the loading jack and the simulated diaphragm connection were mounted on an A-frame structure that resisted the force couple of the jack and diaphragm. Uplift resistance against these forces was provided by anchoring the A-frame structure to the concrete slab.

19448201, 2026, 2, Downloaded from https://onlinelibrary.wiley.com/doi/10.1002/eqs4.70065 by University Of Auckland, Wiley Online Library on [24/06/2026]. See the Terms and Conditions (https://onlinelibrary.wiley.com/terms-and-conditions) on Wiley Online Library for rules of use; OA articles are governed by the applicable Creative Commons License



FIGURE 4 | Cross-section of single-wythe wall showing a vertically installed mechanical anchor (typ.) embedded in heritage brick parapet, with installation process and final positions shown on right (photos supplied by PYTHON Fasteners USA).

TABLE 2 | Masonry and mortar material properties.

Masonry material	Compressive strength	CoV	Estimated tensile strength by 5% of compressive strength
Vintage bricks	17.80 MPa (2580 psi)	0.40	0.9 MPa (130 psi)
Group 1 mortar (G1-1, G1-2)	0.40 MPa (58 psi)	—	Negligible
Group 2 mortar (G2-1 to G2-6)	4.60 MPa (710 psi)	0.18	0.23 MPa (36 psi)
Group 3 mortar (G3-1 to G3-13)	9.70 MPa (1400 psi)	0.30	0.5 MPa (70 psi)

With the diaphragm and parapet base restrained against lateral movement but allowed to rotate, the loads applied on the parapet wall were analogous to a three-point bending setup. This resulted in an effectively determinate system where the horizontal reactions at the diaphragm and parapet foot could be calculated statically using the location of the applied lateral load. Loading of the specimens was conducted either monotonically or cyclically. Figure 3b shows the two possible directions for monotonic loading (i.e., either away from the diaphragm [“push”] or toward the diaphragm [“pull”]). There is currently no standardized testing protocol specifically addressing out-of-plane cyclic loading of masonry. Therefore, the procedure outlined in ASTM E2126-19 Test Method B (ASTM 2019) and FEMA 461 Protocol I – Quasi-Static Cyclic Deformation Controlled Testing (FEMA 2007) was adopted as a reference for designing the testing sequence. The loading protocol was displacement-controlled involving incrementally increasing target displacement amplitudes. At each target displacement, two fully reversed loading cycles were applied. For specimens G3-7a, G3-7b, G3-12, and G3-13, target displacements were increased in 5 mm (0.2 in) increments, while the remaining specimens were tested using 10 mm (0.4 in) displacement increments.

The mechanical anchors were installed by first hammer drilling a pilot hole through the full parapet height at locations that avoided vertical mortar joints. Hammer drilling is generally discouraged in heritage URM due to the potential for local damage to bricks or mortar. However, in this study, the use of rotary hammer drilling was necessary to enable installation of the long mechanical anchors, for which no alternative technique was practically feasible. Previous research

19448201, 2026, 2, Downloaded from https://onlinelibrary.wiley.com/doi/10.1002/eqs4.70065 by University Of Auckland, Wiley Online Library on [24/06/2026]. See the Terms and Conditions (https://onlinelibrary.wiley.com/terms-and-conditions) on Wiley Online Library for rules of use; OA articles are governed by the applicable Creative Commons License

by Galvez et al. (2024) demonstrated that such drilling can cause radial cracking and brick blowout in cavity walls, leading to a local reduction in capacity. In contrast, for the vertical drilling investigated herein, no blowout is expected and only minor radial cracking may occur.

Drilling the vertical pilot holes with a handheld drill and no guiding system proved impractical, as maintaining drill-bit verticality often caused the bit to deflect and blow out through the side of the wall. To ensure accurate alignment of the holes, and therefore of the installed anchors, a drilling guide was used (see Figure 4). The guide consisted of a steel plate with four supports that could be adjusted and temporarily fixed to the top of the wall to level the plate and hold it in place during drilling. A steel pipe was welded perpendicular to the plate that provided a rigid guide to insert the drill bit, ensuring consistent verticality throughout drilling. Due to the long hole depth, dust needed to be extracted at regular intervals using a vacuum and a thin pipe to proceed smoothly with the drilling. After drilling the pilot hole, anchors were installed using a 1000 Nm (0.74 kip-ft) torque impact driver, inducing a compressive confinement that can be assumed to compensate for any local strength reduction associated with drilling-induced damage. The parapet specimens were first tested without these mechanical anchors and later retrofitted with mechanical anchors to observe the increase in lateral strength.

5.1 | Testing Parapets in As-Built Condition to Induce Cracks

It is commonly assumed in analysis of URM parapets that the mortar layer directly above the roof diaphragm is fully cracked due to the generally long service life over which they have been subjected to weather deterioration and minor seismic shaking events. Additionally, some buildings have waterproofing membranes or flashings that are inserted between bricks at the roof diaphragm elevation to prevent the ingress of rainwater. When this condition is present or the parapet is assumed to be cracked, resistance against seismic loading is assumed to be provided purely by the postcracked rocking strength of the URM parapet above (ASCE 2023).

To replicate cracked field conditions, the parapet in its uncracked as-built state is loaded monotonically or cyclically until a horizontal flexure crack is induced at the diaphragm. Table 3 compiles the lateral loads required to reach the precracked strength and subsequent postcracked rocking strength for each parapet specimen. The loads are normalized by the effective height of the parapet wall from the diaphragm to the point of load application by reporting the bending moment at the diaphragm. The dataset for Group 3 mortar shows an average precracked moment strength of 3.72 kNm (2.7 kip-ft) with an associated CoV of 0.2. This corresponds to a flexure tensile strength of 0.4 MPa (0.06 ksi) when applying the classical equation relating bending moments (M) to stresses (σ) along an uncracked section of $\sigma = My/I$, where y is the distance to the uncracked neutral axis and I is the moment of inertia of the uncracked section relative to its neutral axis. This was close to the estimated tensile strength (f_{tm}) for the mortar of 0.5 MPa (0.07 ksi) or 5% f_{cm} as reported in Table 2. In comparison, the lateral load capacity of the parapets after cracking is much less than the as-built strength and would require retrofit in areas of even medium seismicity to prevent collapse.

6 | Experimental Test Results

The results of all the parapet tests are presented in Figures 5–8. Table 4 tabulates the test results including peak lateral load as the minimum from either push or pull direction of loading, base shear coefficient (peak horizontal load P divided by self-weight W), associated peak displacement, direction of loading at failure, and the recorded failure mode that refers to the image and diagrams included in Figure 9. Results generally show that the push direction was stiffer, and failure resulted in this loading direction in the cyclic load protocol.

7 | Observed Failure Mechanisms

When no anchors are installed in the parapet wall and the specimen is loaded at the top of the wall, failure is characterized by a single horizontal crack at a load corresponding to the mortar's precracked strength. Further loading results in a simple rocking mechanism as there is effectively no connection between the two rigid bodies above and below the horizontal crack. To ensure adequate continuity between vertical and horizontal anchors, the diaphragm anchors were evenly spaced with a separation equal to or less than one brick length, while the maximum spacing of vertical anchors was limited to three brick lengths to avoid potential issues with effective width. By maintaining these two conditions, the system provided sufficient continuity between vertical and horizontal anchors, ensuring consistent structural performance of the strengthened parapet.

19448201, 2026, 2, Downloaded from https://onlinelibrary.wiley.com/doi/10.1002/eqs4.70065 by University Of Auckland, Wiley Online Library on [24/06/2026]. See the Terms and Conditions (https://onlinelibrary.wiley.com/terms-and-conditions) on Wiley Online Library for rules of use; OA articles are governed by the applicable Creative Commons License

TABLE 3 | Summary of as-built parapet precracked and postcracked rocking strengths.

Parapet test	Mortar group	Height above diaphragm	Precracked strength and lateral load and moment (kN, kip) | (kNm, kip-ft)		Postcracked rocking strength and lateral load and moment (kN, kip | kNm, kip-ft)	
PL1-S1	G1	500 mm (19.7″)	0.6 kN (0.1 kip)	0.3 kNm (0.2 kip-ft)	0.6 kN (0.1 kip)	0.3 kNm (0.2 kip-ft)
PM1-S1	G2	500 mm (19.7″)	—	—	0.2 kN (0.04 kip)	0.1 kNm (0.1 kip-ft)
PM2-S1	G2	500 mm (19.7″)	4.2 kN (0.9 kip)	2.1 kNm (1.5 kip-ft)	0.7 kN (0.2 kip)	0.4 kNm (0.3 kip-ft)
PM3-S1	G2	1010 mm (39.8″)	—	—	—	—
PH1-S1	G3	650 mm (25.6″)	4.4 kN (1.0 kip)	2.9 kNm (2.1 kip-ft)	0.6 kN (0.1 kip)	0.3 kNm (0.2 kip-ft)
PH2-S1	G3	650 mm (25.6″)	5.5 kN (1.2 kip)	3.6 kNm (2.6 kip-ft)	—	—
PH3-S1	G3	650 mm (25.6″)	6.7 kN (1.5 kip)	4.4 kNm (3.2 kip-ft)	1.3 kN (0.3 kip)	0.9 kNm (0.7 kip-ft)
PH4-S1	G3	650 mm (25.6″)	7.8 kN (1.8 kip)	5.1 kNm (3.8 kip-ft)	0.7 kN (0.2 kip)	0.4 kNm (0.3 kip-ft)
PH5-S1	G3	900 mm (35.4″)	2.9 kN (0.7 kip)	2.7 kNm (2.0 kip-ft)	0.6 kN (0.1 kip)	0.5 kNm (0.4 kip-ft)
PH6-S1	G3	400 mm (15.7″)	9.6 kN (2.2 kip)	3.8 kNm (2.8 kip-ft)	0.8 kN (0.2 kip)	0.3 kNm (0.2 kip-ft)
PH7-S1	G3	650 mm (25.6″)	1.0 kN (0.2 kip)	0.6 kNm (0.4 kip-ft)	1.0 kN (0.2 kip)	0.6 kNm (0.4 kip-ft)

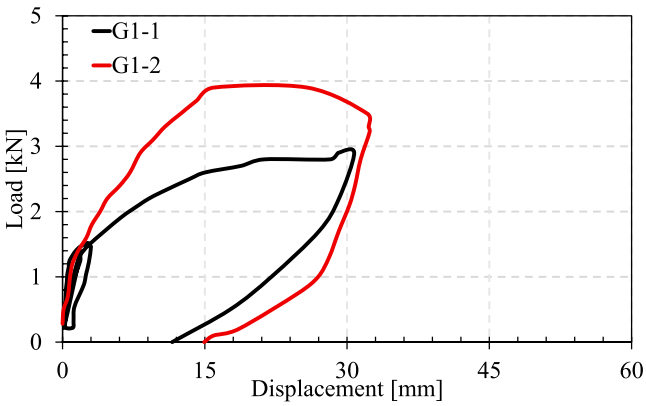


FIGURE 5 | Load displacement relations for Group 1 (G1) parapets.

Retrofitting the parapets with mechanical anchors in a variety of configurations resulted in 25 unique tests. Of the 25 unique tests conducted on the parapet specimens, predominantly four failure mechanisms were observed. The failure mechanisms are presented in Figure 9. Splitting of the anchor has not been represented in Figure 9 as the anchor fracture inside the parapet and was not accessible.

Figure 9a shows a failure characterized by a horizontal crack such that the specimen reverts to a rocking mechanism. This failure is closely related to the mortar precracked strength and the bending moment gradient below the diaphragm. When anchors are not present, the parapet will crack in flexure at the point of highest moment, typically at the diaphragm connection. If anchors are present but the anchor embedment versus diaphragm elevation ratio is small, flexural cracking

19448201, 2026, 2, Downloaded from https://onlinelibrary.wiley.com/doi/10.1002/eqs4.70065 by University Of Auckland, Wiley Online Library on [24/06/2026]. See the Terms and Conditions (https://onlinelibrary.wiley.com/terms-and-conditions) on Wiley Online Library for rules of use; OA articles are governed by the applicable Creative Commons License

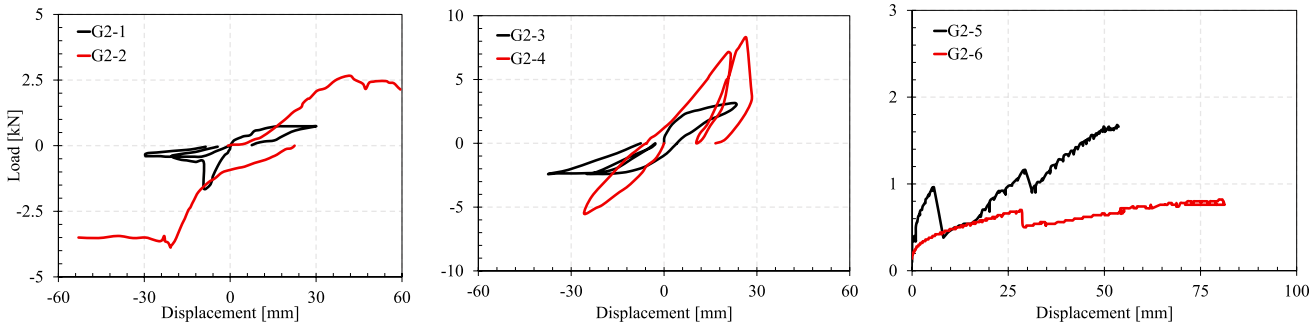


FIGURE 6 | Load displacement relations for Group 2 (G2) parapets.

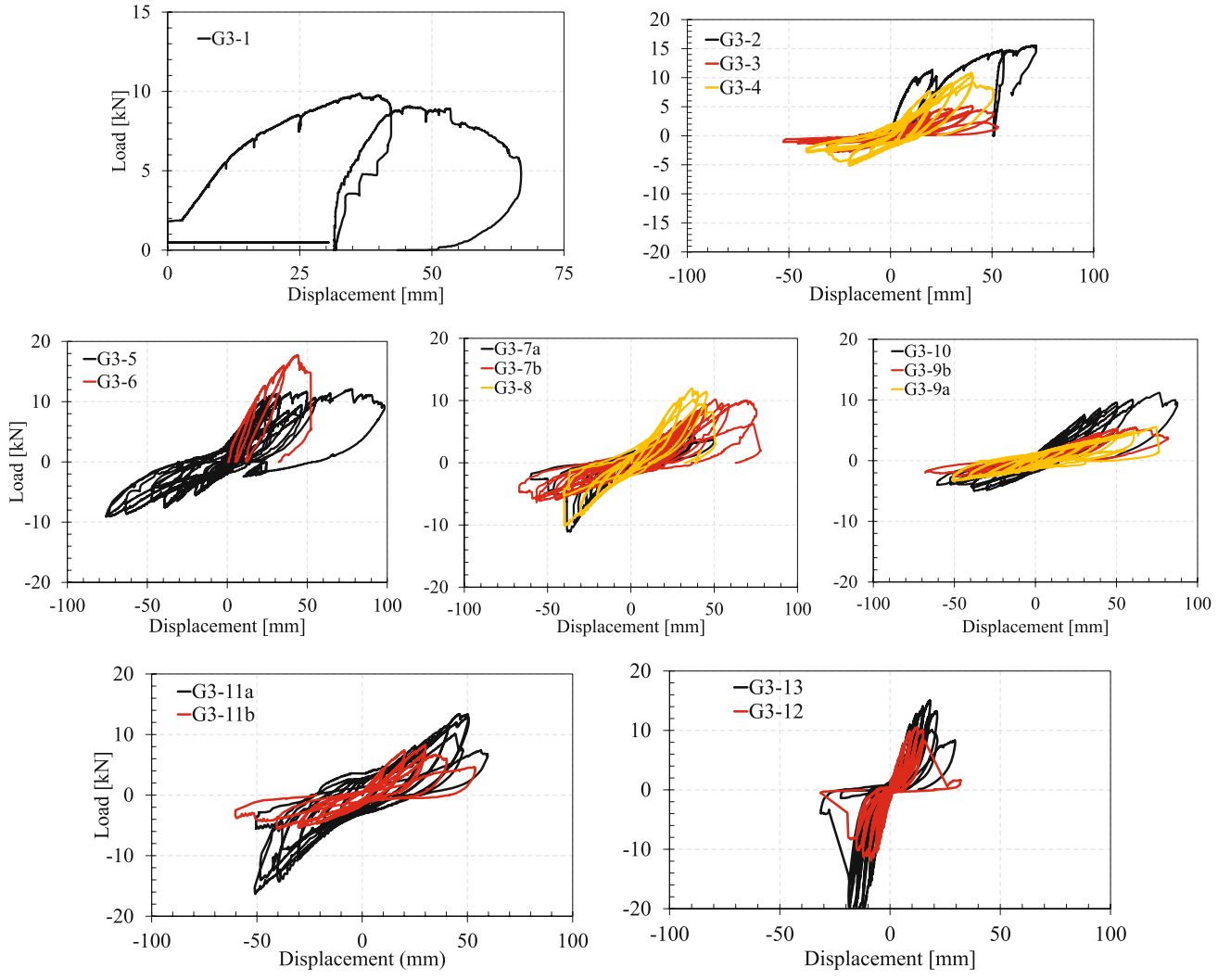


FIGURE 7 | Load displacement relations for Group 3 (G3) parapets.

through an unreinforced mortar layer below the anchor's embedded depth can also occur, resulting in a brittle failure. This failure was observed exclusively in tests where strongbacks were omitted, suggesting that strongbacks can provide effective restraint against flexural mortar cracking in layers below the diaphragm. Analysis of cracked sections also suggests that increased anchor embedment can effectively restrain this type of failure mode. It should be noted that when only long anchors are installed, the crack may form at the top of the piers of the floor immediately below the parapet with the parapet rotating around the diaphragm (see Figure 9d). In such cases, the affected pier will be precracked at its upper end, which needs to be considered in the in-plane assessment of the pier.

19448201, 2026, 2, Downloaded from https://onlinelibrary.wiley.com/doi/10.1002/eqs4.70065 by University Of Auckland, Wiley Online Library on [24/06/2026]. See the Terms and Conditions (https://onlinelibrary.wiley.com/terms-and-conditions) on Wiley Online Library for rules of use; OA articles are governed by the applicable Creative Commons License

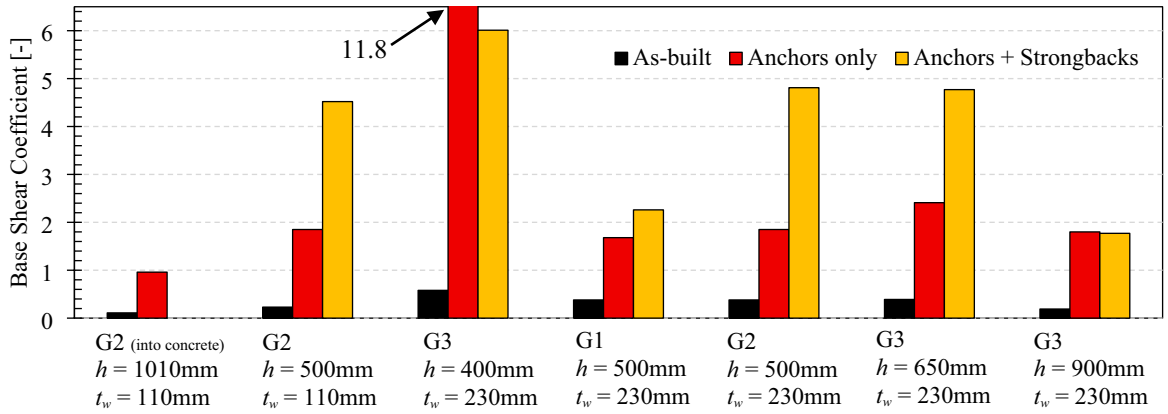


FIGURE 8 | Impact of test variables on the measured lateral strength of parapet specimens. The base shear coefficient is defined as the ratio of peak horizontal load and the parapet self-weight.

Figure 9b shows a splitting pullout failure of the vertical anchors, as shown by the vertical cracks in the exposed mechanical anchors. This failure mode was predominantly observed in two-wythe parapets where the internal lever arm was sufficiently large to generate large steel forces and accounted for most of the observed failures. Tests suggest that pullout is the governing mechanism for two-wythe parapets if reinforced with less than three mechanical anchors per meter of parapet wall. As the process of anchors pulling out from below the diaphragm was not associated with sudden or significant strength loss, failure was generally ductile.

Investigation into fracture failure showed that the protype anchors would fail at the welded segments. This was typically observed in the two wythe parapets where the internal lever arm and depth of compression, as determined by sectional bending analysis, is sufficiently large such that anchor fracture is critical. When the parapet is perched on a concrete slab, this mechanism, brick crushing, and breakout of the anchors from the concrete govern the flexural strength since pullout and horizontal cracking do not apply. Failure generally lacked ductility and was characterized by the sound of steel rupturing. Postfailure loading suggests that the parapet wall had reverted to its postcracked rocking strength, as there was no longer a connection between the top of the parapet wall and the remaining segment below. It is noted that all tests were conducted using prototype anchors with welded segments and that failure by anchor fracture will likely be at higher strength and more ductile when continuous anchors with no weak welded segments are used.

Figure 9c shows failures where the brick and mortar reached their compressive strengths and crushed. The mortar was typically weaker than the brick, resulting in the mortar crushing first and subsequent brick crushing in regions where loads were concentrated in the brick. Analysis by sections show that this failure mode is more critical in one-wythe parapets due to the smaller internal lever arm and larger relative reinforcement ratio. Experimental evidence supports this claim, as most of the one-wythe parapet tests in a previous experiment series failed in such a manner. Failure by brick crushing had some ductility but was not as ductile as failure by anchor pullout.

Failure was always observed in the "push" direction when anchor pullout was observed and never in the "pull" direction. As the observed failure was typically flexural in nature, the preference for failure in the "push" direction may be due to the diaphragm connection. Under flexural actions, the vertical anchors act in tension to pull out of the wall below the diaphragm, introducing splitting stresses along the width of the wall as denoted by σ_A in Figure 10. When the parapet is loaded away from the diaphragm, the diaphragm connection is provided purely by the diaphragm anchors acting in tension to restrain the parapet. This also introduces local splitting stresses in the vicinity of the diaphragm anchors. The direction of these splitting stresses coincides with the direction of splitting stresses due to pullout of the vertical flexure anchors (see Figure 10). In contrast, loading in the "pull" direction whereby the parapet is loaded toward the diaphragm puts the diaphragm connection to URM parapet in compression, resulting in more even distribution of forces and no significant splitting stresses.

8 | Effectiveness of Mechanical Anchors on Lateral Load Capacity

As there is a high likelihood that URM parapets in service are cracked at their base, the increase in strength when mechanical fixings are installed in the parapet specimens is compared against the postcracked rocking capacity. The

19448201, 2026, 2, Downloaded from https://onlinelibrary.wiley.com/doi/10.1002/eqs4.70065 by University Of Auckland, Wiley Online Library on [24/06/2026]. See the Terms and Conditions (https://onlinelibrary.wiley.com/terms-and-conditions) on Wiley Online Library for rules of use; OA articles are governed by the applicable Creative Commons License

TABLE 4 | Summary of parapet test results.

Test ID	Parapet name	Peak lateral load (P) [kN, kip]	Base shear coefficient (P/W)	Associated peak displacement (Δ) [mm, in]	Direction of loading at peak	Failure modes
G1-1	#PL1-S2	2.9 kN (0.7 kip)	1.7	30.7 mm (1.21″)	Push	Flexural mortar cracking
G1-2	#PL1-S3	3.9 kN (0.9 kip)	2.3	15.9 mm (0.63″)	Push	Splitting/pullout
G2-1	#PM1-S2	1.6 kN (0.4 kip)	1.9	9.2 mm (0.36″)	Pull	Flexural mortar cracking
G2-2	#PM1-S3	3.9 kN (0.9 kip)	4.5	20.8 mm (0.82″)	Pull	Pullout/brick crushing
G2-3	#PM2-S2	3.2 kN (0.7 kip)	1.9	22.8 mm (0.90″)	Push	Flexural mortar cracking
G2-4	#PM2-S3	8.3 kN (1.9 kip)	4.8	26.6 mm (1.05″)	Push	Splitting/pullout + brick crushing
G2-5	#PM3-S2	0.8 kN (0.2 kip)	1.0	95 mm (3.74″)	Push	Brick crushing
G2-6	#PM3-S3	1.7 kN (0.4 kip)	0.5	57 mm (2.24″)	Push	Brick crushing
G3-1	#P1-S4	9.9 kN (2.2 kip)	4.4	36.2 mm (1.43″)	Push	Splitting/pullout
G3-2	#P2-S2	15.4 kN (3.5 kip)	6.8	71.5 mm (2.81″)	Push	Splitting/pullout
G3-3	#P2.1-S1	5.1 kN (1.1 kip)	2.3	40.3 mm (1.59″)	Push	Splitting/pullout
G3-4	#P2.2-S2	10.9 kN (2.4 kip)	7.9	39.9 mm (1.57″)	Push	Splitting/pullout
G3-5	#P3-S2	12.1 kN (2.7 kip)	5.4	78.1 mm (3.07″)	Push	Splitting/pullout
G3-6	#P3.1-S1	17.6 kN (4.0 kip)	12.7	44.4 mm (1.75″)	Push	Anchor fracture
G3-7a	#P4-S2	5.4 kN (1.2 kip)	2.4	37.8 mm (1.59″)	Push	Flexural mortar cracking below anchors
G3-7b	#P4-S3	10.1 kN (2.3 kip)	4.5	51.0 mm (2.00″)	Push	Splitting/pullout
G3-8	#P4.1-S1	11.9 kN (2.7 kip)	8.6	36.7 mm (1.44″)	Push	Splitting/pullout + brick crushing
G3-9a	#P5-S2	5.6 kN (1.3 kip)	1.8	74.5 mm (2.93″)	Push	Flexural mortar cracking below anchors
G3-9b	#P5-S3	5.5 kN (1.2 kip)	1.8	61.8 mm (2.43″)	Push	Splitting/pullout
G3-10	#P5.1-S1	11.2 kN (2.5 kip)	5.0	67.7 mm (2.67″)	Push	Splitting/pullout
G3-11a	#P6-S2	16.3 kN (3.7 kip)	11.8	50.8 mm (2.00″)	Pull	Splitting/pullout + flexural mortar cracking below anchors

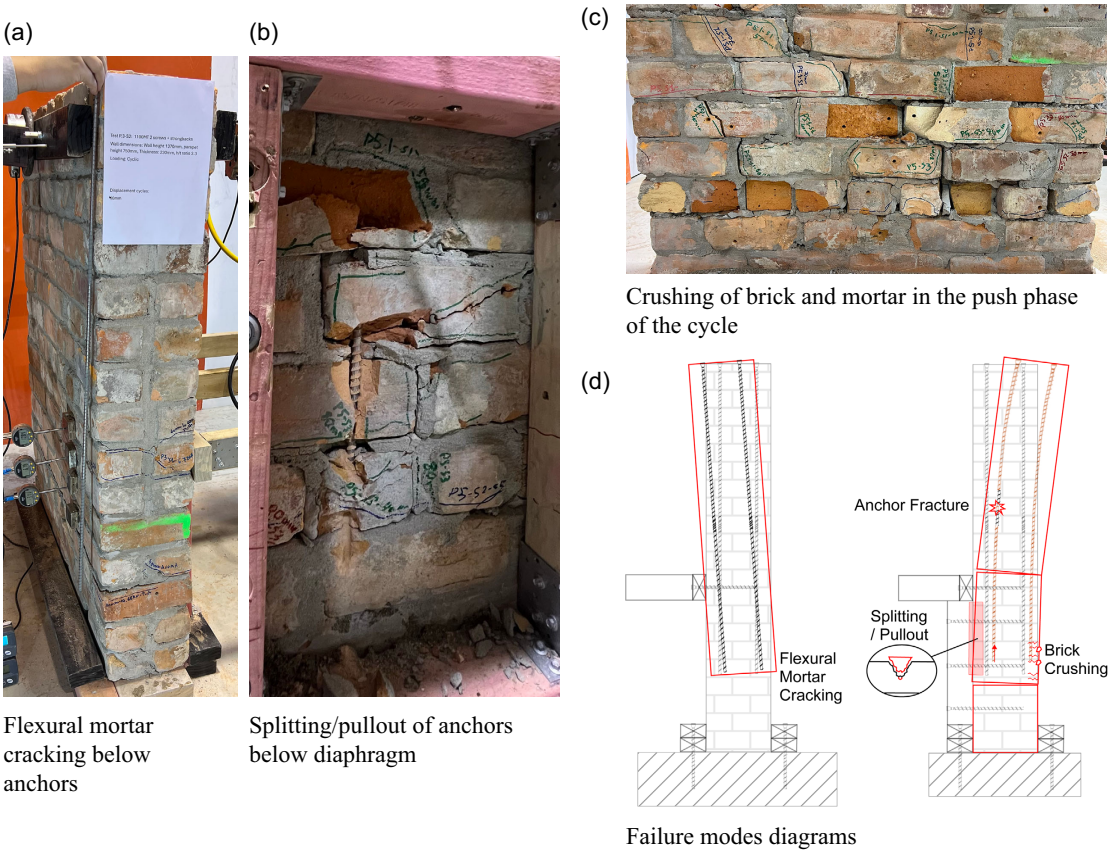
(Continues)

19448201, 2026, 2, Downloaded from https://onlinelibrary.wiley.com/doi/10.1002/eqs4.70065 by University Of Auckland, Wiley Online Library on [24/06/2026]. See the Terms and Conditions (https://onlinelibrary.wiley.com/terms-and-conditions) on Wiley Online Library for rules of use; OA articles are governed by the applicable Creative Commons License

TABLE 4 | (Continued)

Test ID	Parapet name	Peak lateral load (*P*) [kN, kip]	Base shear coefficient (*P/W*)	Associated peak displacement (Δ) [mm, in]	Direction of loading at peak	Failure modes
G3-11b	#P6-S3	8.3 kN (1.9 kip)	6.0	30.0 mm (1.18″)	Push	Splitting/pullout
G3-12	#P7-S2	12.4 kN (2.8 kip)	5.5	10.5 mm (0.41″)	Pull	Anchor fracture
G3-13	#P7-S3	21.5 kN (4.8 kip)	9.6	17.9 mm (0.70″)	Pull	Concrete breakout[a]

[a]Concrete breakout not considered in design equations.



Flexural mortar cracking below anchors

Splitting/pullout of anchors below diaphragm

Crushing of brick and mortar in the push phase of the cycle

Failure modes diagrams

FIGURE 9 | Observed failure modes. (a) Flexural mortar cracking below anchors. (b) Splitting/pullout of anchors below diaphragm. (c) Crushing of brick and mortar in the push phase of the cycle. (d) Failure modes diagrams.

specimens were first tested for their cracked and postcracked rocking strength, and then, mechanical anchors were installed to assess their lateral strength. For some specimens, loading was first applied with installed anchors but no strongbacks to observe the strongback's effects on the failure mechanics and then retested with the strongbacks in place to observe the recovery in lateral load capacity.

A high-level overview of the strength increase due to mechanical anchors is presented in Figure 11, which presents the lateral strength of the parapet wall with and without anchors attached. Additionally, the response of the anchors is separated by specimens with and without strongbacks to understand its effect on the lateral load capacity. It is observed that anchors are highly effective, irrespective of whether strongbacks are present, in increasing the lateral capacity of the parapet walls. For all specimens, the lateral load capacity increased a minimum of 5 times the postcracked rocking strength and up to 25 times larger than the postcracked rocking strength.

19448201, 2026, 2, Downloaded from https://onlinelibrary.wiley.com/doi/10.1002/eqs4.70065 by University Of Auckland, Wiley Online Library on [24/06/2026]. See the Terms and Conditions (https://onlinelibrary.wiley.com/terms-and-conditions) on Wiley Online Library for rules of use; OA articles are governed by the applicable Creative Commons License

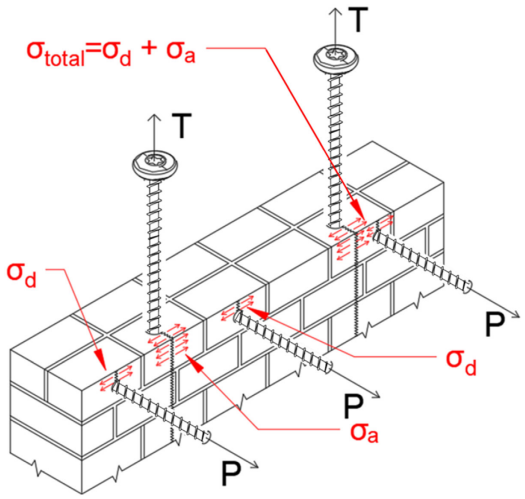


FIGURE 10 | Combined effect of anchor pullout and diaphragm anchors on vertical splitting cracks.

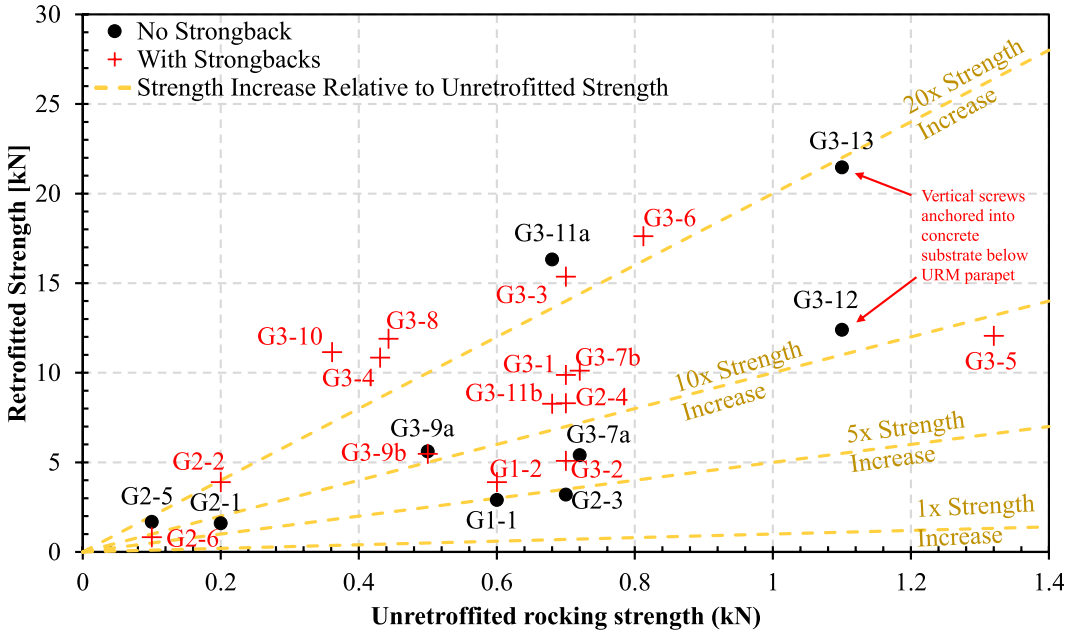


FIGURE 11 | Impact of the presence/absence of wooden strongbacks on the lateral load capacity amplification in parapet specimens retrofitted with anchors.

8.1 | Effects of Strongbacks on Lateral Capacity

Most of the experimental data summarized in Figure 11 were conducted with strongbacks, but Test IDs G3-7, G3-9, and G3-11 were first tested without strongbacks, and then, strongbacks were installed to observe its effects on cyclic behavior. The specific geometry of each test and results can be found in Tables 3 and 4.

Test ID G3-7, which is nominally identical to Test IDs G3-1 and G3-5 in parapet geometry, anchoring configuration, and materials, showed that a horizontal crack tended to form below the anchor's embedment if no strongbacks are present. This resulted in a lower lateral capacity of about 5 kN (1.1 kip). When strongbacks were installed to strengthen the wall below the diaphragm, the specimen regained its strength to be on par with Test IDs G3-1 and G3-5 at approximately 10 kN (2.2 kip). This test suggested that parapet walls without strongbacks may fail at a reduced load due to flexure cracking in regions below the effective anchor embedment, which is related to the anchor embedment and diaphragm elevation (see Figure 9a). The remaining tests also suggested that strongbacks effectively strengthen the wall below the diaphragm elevation such that failure by flexure cracking in regions without vertical anchors will not govern the lateral capacity.

19448201, 2026, 2, Downloaded from https://onlinelibrary.wiley.com/doi/10.1002/eqs4.70065 by University Of Auckland, Wiley Online Library on [24/06/2026]. See the Terms and Conditions (https://onlinelibrary.wiley.com/terms-and-conditions) on Wiley Online Library for rules of use; OA articles are governed by the applicable Creative Commons License

Test IDs G3-9 and G3-11 further clarified the role of strongbacks in lateral strengthening. It was observed that there was no difference in strength between the tests with and without strongbacks for Test ID G3-9. This was attributed to the interaction between the anchor embedment length, effective wall height, and diaphragm elevation. Test ID G3-9 had the largest ratio between anchor embedment and diaphragm elevation, which increases the lateral load capacity corresponding to flexure cracking in unreinforced regions. Test ID G3-9 also had the largest effective height, which means that larger bending moments are applied at the diaphragm elevation per unit lateral load. This reduces the lateral load capacity corresponding to the pullout or fracture strength of the mechanical anchors. The combination of increased precracked capacity in unreinforced regions and reduced lateral anchor capacity resulted in the test without strongbacks failing by cracking below the mechanical anchors. Subsequently, repairs by installing strongbacks resulted in a similar lateral capacity and failure by flexural pullout of mechanical anchors.

Test ID G3-11 demonstrated a greater capacity without strongbacks than with strongbacks. Similar principles of effective height, anchor embedment, and diaphragm elevation in Test ID G3-9 also influenced the lateral capacity of Test ID G3-11. While Test ID G3-11 had the same anchor embedment-to-diaphragm elevation ratio as G3-9, it had the shortest effective height, resulting in greater shear demand relative to moment demand. The reduced flexure demand and larger shear demands meant that the relative contribution of diaphragm anchors to brick vertical splitting was larger when compared with previous tests. This resulted in the lateral capacity associated with lateral pullout being close to the flexure mortar cracking capacity.

Testing showed that splitting pullout occurred first. As this mechanism was relatively ductile and allowed for minor strength gain, horizontal cracking was subsequently observed in the region below the anchors. In this case, repairs with strongbacks did not recover lateral strength, because strongbacks did not repair the pullout capacity of anchors.

8.2 | Effects of Loading Protocol and Repeatability

The tested behaviors of Test IDs G3-1, G3-3, and G3-4 are presented in Figure 12. These three parapets are nominally identical with the same number of anchors and effective anchor depth and were loaded at the same effective height in either monotonic or cyclic load protocols. The monotonic envelope from Test ID G3-1 is overlain on the cyclic responses of Test IDs G3-3 and G3-4. G3-3 had a typical anchor spacing of 500 mm (19.7 in.) in the 1.0 m (39.4 in.) wide parapet wall (approx. 2 bricks lengthwise), while G3-4 had a larger anchor spacing of about 700 mm (27.6 in) (approx. 3 bricks) in the 1.0 m (39.4 in) wide parapet wall.

Failure in all three specimens presented occurred in the push direction, as that was the stiffer and weaker direction when strongbacks were installed below the diaphragm. The increase in lateral strength following retrofit with anchors was quite consistent, with the lateral load capacity increasing from about 1 kN (0.22 kip) to peak strengths between 10 kN (2.2 kip) and 12 kN (2.7 kip). Failure was generally ductile, with the yielding mechanism characterized by vertical splitting cracks at the location of the installed anchors. There was no observed degradation in capacity in the cyclic loading protocol when compared to the monotonic load protocol, suggesting that failure is driven by pullout of the anchors as this is a relatively ductile failure mode.

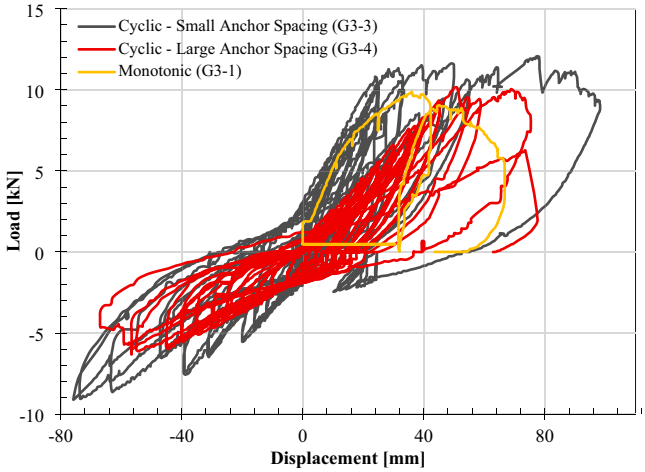


FIGURE 12 | Monotonic and cyclic behavior of geometrically identical parapets with varying anchor reinforcement configurations (G3-1, G3-3, and G3-4).

19448201, 2026, 2, Downloaded from https://onlinelibrary.wiley.com/doi/10.1002/eqs4.70065 by University Of Auckland, Wiley Online Library on [24/06/2026]. See the Terms and Conditions (https://onlinelibrary.wiley.com/terms-and-conditions) on Wiley Online Library for rules of use; OA articles are governed by the applicable Creative Commons License

As the lateral capacity is controlled by the capacity of the anchors and associated pullout strength, there was little difference in the peak strength among the three specimens. However, there is a noticeable difference in the load-displacement response when comparing the specimen with normal anchor spacing and large anchor spacing. The reduced stiffness in the test with larger anchor spacing may imply that there is a reduction in effective parapet width when the anchor spacing is large or the edge distance is small. To specify a detailed relationship between anchor spacing and influential parapet parameters would require further testing beyond the scope of the present study. However, the parapet configuration #P4-S3 had a larger anchor spacing and hence a lower side of the wall edge distance of 150 mm as compared to the 250 mm of tests P1-S4 and #P3-S2. No reduction in capacity was observed, indicating that the tested anchors are not sensitive to side edge distance within this range. Based on the aforementioned observations and for safe design purposes, it is recommended to limit the maximum anchor spacing to within 3 brick lengths to avoid potential issues with effective width and a minimum edge distance of 150 mm to assure to strength reduction.

8.3 | Effects of Parapet Height on Tension-Controlled Flexure Design

Early observations suggested that the flexural behavior of 1-wythe parapet walls with mechanical anchors is compression-controlled. In contrast, the failure of two-wythe parapet walls with mechanical anchors described was generally tension controlled by the pullout and a lesser extent by the fracture of mechanical anchors. To estimate the anchor forces, the overturning moment generated by the lateral load P over the parapet effective height h is normalized by an assumed internal lever arm of $0.9d$ by Equation (1), where the effective anchor depth (d) is defined as the distance between the compression face and the anchor axis. These results are presented in Figure 13 as functions of the anchor embedment length and effective parapet height-to-depth ratio. The nominal anchor capacity considering the strength of the welded segments is plotted with the dashed red line.

$$T = \frac{Ph}{0.9d} \tag{1}$$

Figure 13a shows the estimated anchor forces as a function of the effective height to wall thickness ratio, where most of the estimated anchor forces were below the nominal anchor capacity in uniaxial tension. The subset of tension-controlled parapets only extended up to an effective height to thickness ratio of 5. Parapets with higher ratios were generally compression controlled. Figure 13b shows the same subset of tension-controlled specimens, with most failing by brick splitting and subsequent anchor pullout. The trends suggest that anchor pullout and subsequent splitting of the brick and mortar is not sensitive to the anchor embedment length. The data also suggests that anchor embedment beyond 300 mm (12″) did not increase the pullout capacity. Based on the results of these tests, it is recommended to extend the mechanical anchors below the diaphragm by 300 mm (12″) where strongbacks are used below the diaphragm level. For configurations associated with higher demand, such as increased wall thickness, increasing the embedment depth beyond

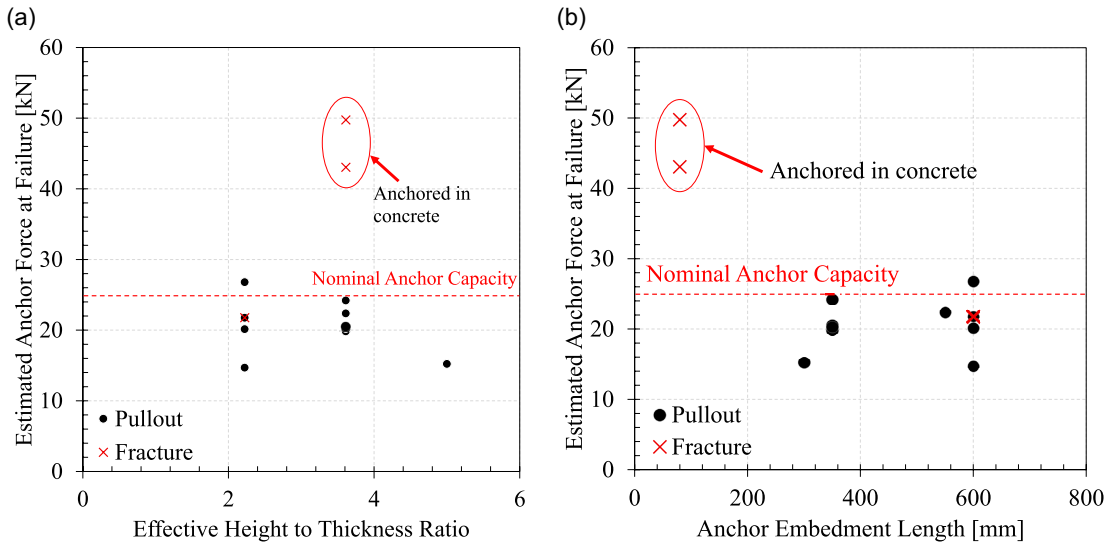


FIGURE 13 | Estimated anchor stresses in tension controlled parapets as a function of (a) effective height to thickness ratio and (b) anchor embedment length.

19448201, 2026, 2, Downloaded from https://onlinelibrary.wiley.com/doi/10.1002/eqs4.70065 by University Of Auckland, Wiley Online Library on [24/06/2026]. See the Terms and Conditions (https://onlinelibrary.wiley.com/terms-and-conditions) on Wiley Online Library for rules of use; OA articles are governed by the applicable Creative Commons License

the recommended value may not result in a proportional increase in system capacity. However, the methodology proposed in the following section allows the designer to verify whether additional embedment is required for a given demand. Additional embedment may also be considered if site conditions limit the use of strongbacks and the URM wall is susceptible to flexure cracking between stories.

The red dashed line indicating the nominal anchor capacity is obtained via uniaxial tension test, with the strength limited by fracture of the welded segments in the anchor. The figure shows that the estimated anchor force upon reaching the lateral capacity is generally below the nominal anchor fracture capacity, suggesting that anchor yielding or fracture was not controlling. This is consistent with experimental observations where failure was characterized by pullout of the anchors. For specimens failing by anchor fracture, failure occurred at the welded joints. For specimens anchored directly to a concrete slab, failure by fracture was significantly higher than the welded segment's strength and closer to the base metal's strength of 1040 MPa (150.8 ksi), because the welded connections were a significant distance away from the point of highest bending moment at the base of the parapet.

9 | Proposed Approach for Predicting the Lateral Strength of URM Parapets Retrofitted With Mechanical Anchors

This section seeks to leverage the presented experimental observations and data to develop a practical approach for predicting the lateral strength of URM parapets retrofitted with mechanical anchors. The out-of-plane response of the parapet is governed by flexure, resulting in different failure modes. The system capacity is controlled by both the tensile capacity of the mechanical anchors installed in the masonry and the capacity of the masonry to bend and crush. In the context of ASCE/SEI 41-23, these are treated as force-controlled actions. The recorded capacities are independent of the diaphragm stiffness, hence when designing the retrofit the demands still need to be carefully evaluated in accordance with relevant standards and guidelines considering the stiffness of the structure to design.

Considering the above, a failure mode-based approach was proposed to predict the probable lateral strength of URM parapets retrofitted with mechanical anchors. In this approach, four potential governing failure mechanisms are considered: (1) mortar cracking strength (P_{mt}), (2) mortar crushing (P_{mc}), (3) anchor rupture (P_{ar}), and (4) anchor pullout (P_{ap}). The lateral strength of a URM parapet retrofitted with mechanical anchors can be evaluated as shown in Equation (2).

$$V_n = \min\left(P_{mt}, P_{mc}, P_{ar}, P_{ap}\right) \tag{2}$$

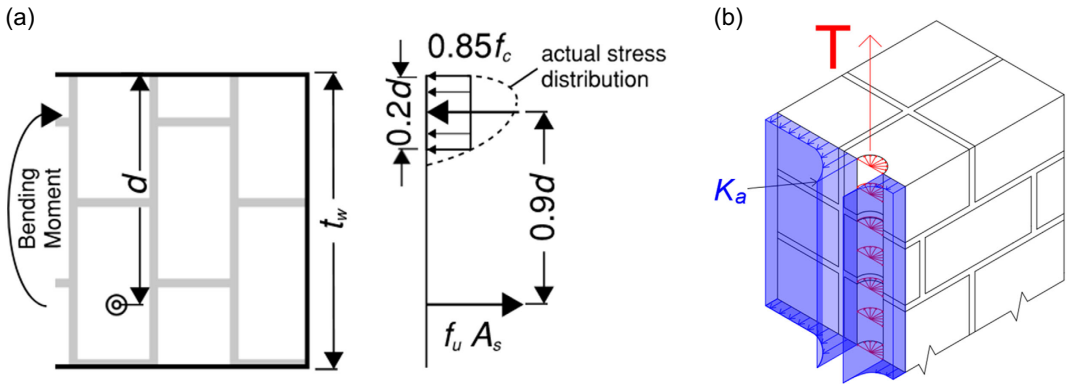
The probable P_{mt} is assumed to be dependent on the mortar tensile strength and the mechanical anchor's embedment length below the diaphragm. The probable P_{mt} can be obtained by setting the moment demand below the diaphragm equal to the flexural capacity. The lateral force corresponding to the moment demand that exceeds the precracked moment capacity is taken as P_{mt}. The bending moment gradient below the diaphragm will vary from building to building depending on the story height and other factors. It is recommended to perform a structural analysis in accordance with ASCE/SEI 41-23 guidelines. Given that this failure mode is undesirable, it can be precluded by installing strongbacks or by extending the mechanical anchor's embedment length. Assuming that URM parapet walls are subject to only inertial forces, engineering judgment suggests that embedding the anchors to half the story height below the diaphragm will effectively suppress mortar cracking, though such a detail may face constructability constraints.

Both P_{mc} and P_{ar} can be derived from the classical section analysis approach. With known geometric quantities such as the effective anchor depth (d), an assumed internal lever arm ($0.9d$), and the in situ material properties, it is possible to provide estimates for the flexural bending strength as governed by anchor rupture and mortar crushing (see Figure 14a). It is recommended to estimate d considering any possible thickness reduction due to the deterioration in the brick or mortar of the parapet. The geometric considerations for deriving the equations for mortar crushing (P_{mc}) and anchor rupture (P_{ar}) are presented in Figure 14a and are expressed by Equations (3) and (4), respectively.

$$P_{mc} = \frac{0.15 d^2 b_{w,eff}}{h} f_{c,min} \tag{3}$$

$$P_{ar} = \frac{0.8 A_s d}{h} f_u \tag{4}$$

19448201, 2026, 2, Downloaded from https://onlinelibrary.wiley.com/doi/10.1002/eqs4.70065 by University Of Auckland, Wiley Online Library on [24/06/2026]. See the Terms and Conditions (https://onlinelibrary.wiley.com/terms-and-conditions) on Wiley Online Library for rules of use; OA articles are governed by the applicable Creative Commons License



Sectional bending strength model for brick crushing and anchor rupture.

Basis of mechanical model for anchor pullout

FIGURE 14 | Mechanical models. (a) Sectional bending strength model for brick crushing and anchor rupture. (b) Basis of mechanical model for anchor pullout.

where d, $b_{w,eff}$, and h refer to the effective thickness, effective width, and effective height as presented previously in Figure 3a. The compressive strength $(f_{c,min})$ should be taken as the lower of the mortar strength (f_{cm}) and brick strength (f_c). To estimate $b_{w,eff}$, it is recommended to assign a reduced effective width of 300 mm (12″) per anchor to account for torsional effects and nonuniformity of the compression zone. In lieu of using this equation, a more detailed sectional analysis using brick-specific and anchor specific stress–strain relations can be used to estimate P_{mc} and P_{ar}.

To estimate the probable P_{ap} associated with anchor pullout by splitting, Figure 14b shows the assumed stress distribution in the brick and mortar for an anchor acting in tension. When an anchor acts in tension, compressive forces (drawn in red) are exerted radially along the anchor diameter. Splitting forces in the brick (drawn in blue) resist the forces and provide equilibrium. When the element to which the anchor is affixed has a sufficiently small thickness, such as that in one-wythe or two-wythe parapet walls, the splitting forces can control the design strength. A stress concentration is typically observed in the brick at its interface with the anchor, as shown in Figure 14b, which can be captured as the average stress times K_a. The anchor force T that causes the splitting stresses to reach the bricks tensile strength f_t at the point of stress concentration is defined as the failure point.

The lateral strength associated with splitting cracks due to anchor pullout is influenced by both longitudinal anchors and diaphragm anchors as previously described by the mechanism in Figure 10. First, the longitudinal anchors are fixed in a vertical orientation, which exerts radial splitting stresses along the length of the parapet wall and makes up the primary contribution to splitting. Second, the anchors securing the parapet to the diaphragm are oriented horizontally, exerting a splitting force in the brick along the length of the parapet wall though to a lesser contribution. The detailed derivation, presented in Appendix A, results in the following equation:

$$P_{ap} = \frac{0.5\pi f_t}{\frac{hK_a}{l_{emb,a}(t_w - D)j_d\left(\frac{b_w}{s_a}\right)} + \frac{K_d}{Dl_{emb,d}\left(\frac{b_w}{s_d}\right)}} \text{(MPa orpsi units)} \quad (5)$$

where f_t is the tensile strength of the brick, t_w is to the total wall thickness, D is the diameter of the mechanical anchor, s_a is the spacing of the longitudinal anchors, s_d is the spacing of the diaphragm anchors, and all other terms as defined previously. Based on the observations for anchor forces at failure as a function of embedment length, it is recommended to take $l_{emb,a} \leq 300$ mm (12 in).

A simplified version of this equation is used by combining several geometric quantities that are similar and the fitted values for K_a and K_p (see Appendix A), resulting in the following equation:

$$P_{ap} = \lambda t_w b_w f_t \quad (6)$$

19448201, 2026, 2, Downloaded from https://onlinelibrary.wiley.com/doi/10.1002/eqs4.70065 by University Of Auckland, Wiley Online Library on [24/06/2026]. See the Terms and Conditions (https://onlinelibrary.wiley.com/terms-and-conditions) on Wiley Online Library for rules of use; OA articles are governed by the applicable Creative Commons License

where λ is taken as

$$\lambda = \frac{0.5}{\frac{hs_a}{dl_{emb,a}} + \frac{s_p}{10D}} \tag{7}$$

9.1 | Validation of Mechanical Model

Equation (2) and the simplified equation for P_{ap} in Equation (6) are used to predict the failure mode and the nominal strength of each test. As shown in Figure 15, the proposed model provides a good estimate of the failure strength of the parapet tests when compared against the unity line, with a coefficient of determination $R^2 = 0.75$, consistent with the level of scatter typically observed in masonry and concrete models. Tests that failed due to flexural mortar cracking were excluded from this comparison, as their predicted capacity depends on the assessment criteria defined in the relevant design standard. In addition, specimens governed by concrete breakout failure were not included, as this failure mode is outside the scope of the proposed design equations. Additionally, as shown in Table 5, the proposed approach accurately predicts the failure mode of 84% of the test specimens.

To account for model uncertainty, for design purposes, a capacity reduction factor (ψ) can be applied on the nominal parapet strength to derive a conservative design strength ψV_n (see Equation (8)).

$$V_u \leq \psi V_n \tag{8}$$

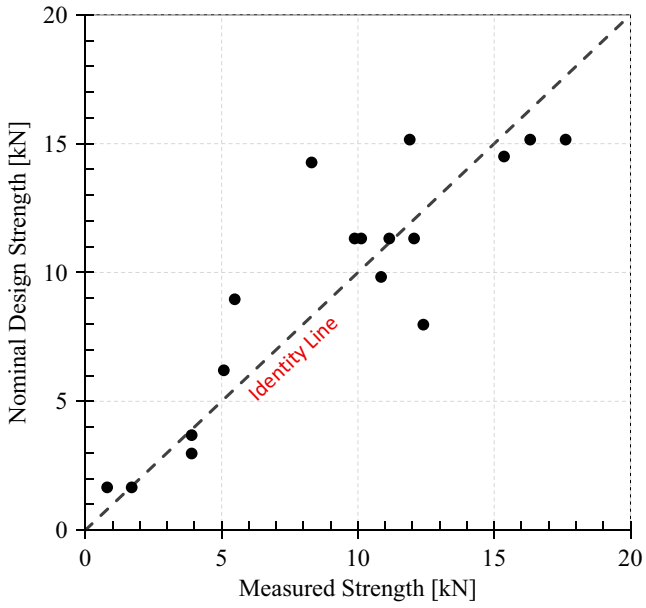


FIGURE 15 | Measured vs. predicted out-of-plane lateral strength of parapet specimens.

TABLE 5 | Confusion matrix for failure mode prediction.

		Predicted failure mode			
		Flexural mortar cracking	**Anchor fracture**	**Anchor pullout**	**Brick crushing**
Experimental failure mode	Flexural mortar cracking	5	0	0	0
	Anchor fracture	0	2	1	0
	Anchor pullout	0	2	10	1
	Brick crushing	0	0	0	4

Note: Green cells indicate correctly predicted failure mechanism.

19448201, 2026, 2, Downloaded from https://onlinelibrary.wiley.com/doi/10.1002/eqs4.70065 by University Of Auckland, Wiley Online Library on [24/06/2026]. See the Terms and Conditions (https://onlinelibrary.wiley.com/terms-and-conditions) on Wiley Online Library for rules of use; OA articles are governed by the applicable Creative Commons License

TABLE 6 | Recommended capacity reduction factors based on target probability of exceedance.

Probability of exceedance	ψ
20%	0.80
15%	0.75
10%	0.70
5%	0.60

where V_n is the nominal parapet lateral strength that considers each failure mechanism as defined by Equation (2) and V_u is the demand lateral load as determined by the applicable code standard such as ASCE 41, which generally consider inertial loads only.

By fitting a normal distribution to the model error of Equation (2), it is possible to select a capacity reduction factor that targets a probability of exceedance. Table 6 presents recommended capacity reduction factors corresponding to the probabilities of exceedance of 5%, 10%, 15%, and 20%, respectively.

10 | Conclusions

This study investigated the effectiveness of postinstalled mechanical anchors for seismic retrofit of URM parapet walls as an alternative to the traditional backstay method. Eleven parapet specimens, spanning multiple geometric and retrofit configurations and tested under monotonic and cyclic loading protocols, were used to evaluate lateral load capacity, failure mechanisms, and design parameters. The test results showed that mechanical anchors significantly improved the lateral load capacity beyond the postcracked rocking strength by a factor between 5 and 25 times. The base shear coefficient was as high as 11.8 when both strongbacks and anchors were used. The effectiveness of the retrofit depends on the anchoring configuration, detailing of the anchor embedment, and presence of strongbacks. The results demonstrated that URM parapet walls can be effectively secured to the roof diaphragm, mitigating collapse risk while avoiding the common downsides of backstays, namely, their impacts on heritage architecture, roof functionality, and compromised waterproofing.

Four critical failure modes were identified, these being horizontal flexure cracking in unreinforced regions, compression failure in flexure, anchor rupture in flexure, and anchor pullout in flexure. Design equations for each of the critical failure modes are provided and calibrated to the test results. The provided equations correctly classified the governing failure mechanism of 84% of the test specimens and has a R^2 value of 0.75. The comparison shows that a good safety margin can be achieved using the provided design equations. A summary and worked example can be found in Appendix B.

Despite the key contributions of the study, there are a few limitations. Edge distance effects for anchors located near wall boundaries were only partially investigated in this study. Future work should focus on combined anchor pull-out and shear behavior when diaphragm anchors are installed close to vertical anchors, as well as the performance of parapets with varying construction materials, wall thicknesses, or nonstandard geometries. Increasing the number of tests per configuration would also enable the calculation of lower-bound capacities for design applications.

Acknowledgments

The authors thank the collaborative efforts of PYTHON Fasteners in generously sponsoring this research and granting access to their products and laboratory facilities. Sandeep Sidhu and Selin Tonnerre are greatly acknowledged for their invaluable help during the testing.

Conflicts of Interest

The authors declare no conflicts of interest.

Data Availability Statement

The data from the experimental research program is wholly reported in this article. For requests regarding information beyond the data provided herein, please contact the authors.

19448201, 2026, 2, Downloaded from https://onlinelibrary.wiley.com/doi/10.1002/eqs4.70065 by University Of Auckland, Wiley Online Library on [24/06/2026]. See the Terms and Conditions (https://onlinelibrary.wiley.com/terms-and-conditions) on Wiley Online Library for rules of use; OA articles are governed by the applicable Creative Commons License

References

ASCE/SEI 41-23. 2023. Seismic Evaluation and Retrofit of Existing Buildings. American Society of Civil Engineers.

ASTM C1329-05. 2005. Specification for Mortar Cement. ASTM International.

ASTM E2126-19. 2019. Test Methods for Cyclic (Reversed) Load Test for Shear Resistance of Vertical Elements of the Lateral Force Resisting Systems for Buildings. ASTM International.

Borri, A., G. Castori, and M. Corradi. 2011. "Shear Behavior of Masonry Panels Strengthened by High Strength Steel Cords." *Construction and Building Materials* 25, no. 2: 494–503.

Bruneau, M. 1995. "Performance of Masonry Structures during the 1994 Northridge (Los Angeles) Earthquake." *Canadian Journal of Civil Engineering* 22, no. 2: 378–402.

California Seismic Safety Commission. 1992. Report No. SSC 92-01 1992 Status of California's Unreinforced Masonry Building Law. Sacremento.

Cassol, D., I. Giongo, J. Ingham, and D. Dizhur. 2021. "Seismic Out-of-Plane Retrofit of URM Walls Using Timber Strong-Backs." *Construction and Building Materials* 269: 121237.

Cassol, D., J. Ingham, and I. Giongo. 2025. "Seismic Out-of-Plane Repair and Strengthening of Masonry Infill Walls Using Timber Strong-Backs." *Structures* 71: 107990.

Dizhur, D., J. Ingham, L. Moon, et al. 2011. "Performance of Masonry Buildings and Churches in the 22 February 2011 Christchurch Earthquake." *Bulletin of the New Zealand Society for Earthquake Engineering* 44, no. 4: 279–296.

Dizhur, D., M. Giaretton, and J. Ingham. 2017. "Seismic Restraint for Clay Brick URM Parapets Validated Using Shake-Table Testing." In *16th World Conference on Earthquake, Chile, 2017*.

Dizhur, D., M. Giaretton, I. Giongo, et al. 2017. "Seismic Retrofit of Masonry Walls Using Timber Strong-Backs." *The Masonry Society Journal* 30: 30–44.

Elgawady, M. 2004. Seismic in-Plane Behavior of URM Walls Upgraded with Composites. EPFL, Lausanne. https://infoscience.epfl.ch/handle/20.500.14299/212441.

Farahani E. M., M. Yekrangnia, M. Rezaie, and R. Bento. 2021. "Seismic Behavior of Masonry Walls Retrofitted by Centercore Technique: A Numerical Study." *Construction and Building Materials* 267: 120382.

FEMA 461. 2007. Interim Testing Protocols for Determining the Seismic Performance Characteristics of Structural and Nonstructural Components.

FEMA 547. 2006. Techniques for the Seismic Rehabilitation of Existing Buildings. Washington D.C.

FEMA E-74. 2012. FEMA E-74 Reducing the Risks of Nonstructural Earthquake Damage - A Practical Guide. Washington D.C.

FEMA P-58. 2018. Seismic Performance Assessment of Buildings. Washington D.C.

FEMA P-1024. 2015. Performance of Buildings and Nonstructural Components in the 2014 South Napa Earthquake. February. Washington, D.C.

Galvez, F., K. Noori, P. Orquillo, et al. 2024. Effects of Drilling Methods on Tensile Capacity of Mechanical Screw Anchors in Masonry Walls. Milan, June 2024.

Giaretton M., D. Dizhur, F. da Porto, and J. M. Ingham. 2016. "Post-Earthquake Reconnaissance of Unreinforced and Retrofitted Masonry Parapets." *Earthquake Spectra* 32, no. 4: 2377–2397.

Giaretton, M., J. Ingham, and D. Dizhur. 2017. "Timber Strong-Backs as Cost-Effective Seismic Rerofit Method for URM Buildings." In *NZSEE Conference, Wellington, New Zealand, February 2017*.

Giaretton, M., D. Dizhur, and J. Ingham. 2018. "Shake Table Testing of Seismically Restrained Clay-Brick Masonry Parapets." *Earthquake Spectra* 34, no. 1: 99–119.

Lourenco, P. 1996. Computational Strategies for Masonry Structures.

Lumantarna, R. 2012. Material Characterisation of New Zealand's Clay Brick Unreinforced Masonry Buildings. University of Auckland.

Mercimek, Ö., M. C. Yılmaz, M. Yasin, et al. 2025. "An Experimental Study about Unreinforced Masonry Panels Strengthening with CFRP: Out-of-Plane Failure." *Engineering Failure Analysis* 181: 109932.

New Zealand Ministry of Business I and E. 2018. Securing Parapets and Facades on Unreinforced Masonry Buildings : Advice for Building Owners, Councils and Engineers. Ministry of Business, Innovation & Employment.

NGDC. 2009. National Hazards Slide Sets. NGDC.

NZSEE C8. 2017. *Unreinforced Masonry Buildings. Epub Ahead of Print*.

Paulay, T., and M. J. N. Priestly. 1992. Seismic Design of Reinforced Concrete and Masonry Buildings. Wiley.

19448201, 2026, 2, Downloaded from https://onlinelibrary.wiley.com/doi/10.1002/eqs4.70065 by University Of Auckland, Wiley Online Library on [24/06/2026]. See the Terms and Conditions (https://onlinelibrary.wiley.com/terms-and-conditions) on Wiley Online Library for rules of use; OA articles are governed by the applicable Creative Commons License

Sommer, D., D. Ash, D. Dizhur, et al. 2019. "Case Study on URM Parapet Bracing: Research and Application." In *13th North American Masonry Conference*.

Tong, Q., O. Filippova, and J. Ingham. 2022. "Effectiveness of Unreinforced Masonry Seismic Retrofit Programmes: Review of Policies in New Zealand and the United States." *International Journal of Disaster Risk Reduction* 76: 103008.

Yılmaz, M. C., A. A. E. Finner, and Ö. Mercimek. 2024. "Experimental Investigation of Out-of-Plane Behaviour of Unreinforced Masonry Panels Strengthened with TRM." *Structures* 65: 106665.

Appendix A

Derivation of Lateral Strength Associated With Anchor Pullout (Equation 2)

The anchor force can be related to the lateral applied load by considering a free-body diagram of the parapet wall above the diaphragm as shown in Figure A1a. Assuming that the internal lever arm is $0.8d$, the anchor force in the vertical anchors is estimated in Equation A-1 as

$$T_1 = \frac{Ph}{0.8d\left(\frac{b_w}{s_a}\right)} \tag{A-1}$$

where P is the lateral load, h is the effective parapet height, d is the effective distance between the compression face to the anchor, and b_w/s_a is the width of the parapet wall divided by anchor spacing, representing the approximate number of anchors in the parapet wall. Likewise, the diaphragm anchors keeping the parapet in horizontal equilibrium is estimated as

$$T_2 = \frac{P}{\left(\frac{b_w}{s_d}\right)} \tag{A-2}$$

where b_w/s_d represents an estimate of the number of diaphragm anchors.

The tensile capacity of the anchors (T) in anchor pullout is related to the splitting stresses in the brick as shown in Figure A1b. Assuming the brick resists the uplifting anchor force uniformly across the embedment depth and apply a compressive stress to the interior of the anchor hole at an angle of 45°, the radial forces applied on the interior of the anchor hole in cylindrical coordinates is

$$\sigma_r(r = D, \theta, z) = \frac{T}{D\pi l_{emb}} \tag{A-3}$$

Integrating in only the horizontal direction gives the total horizontal compressive force exerted by the anchor on the brick, which must equal the tensile force in the brick resisting splitting as shown in Figure A1c. The average splitting force is this force smeared over the corresponding thickness of the brick minus the anchor diameter. With consideration of a stress concentration factor (K_a) at the edge of the anchor hole, the largest splitting stress as a function of the anchor force is

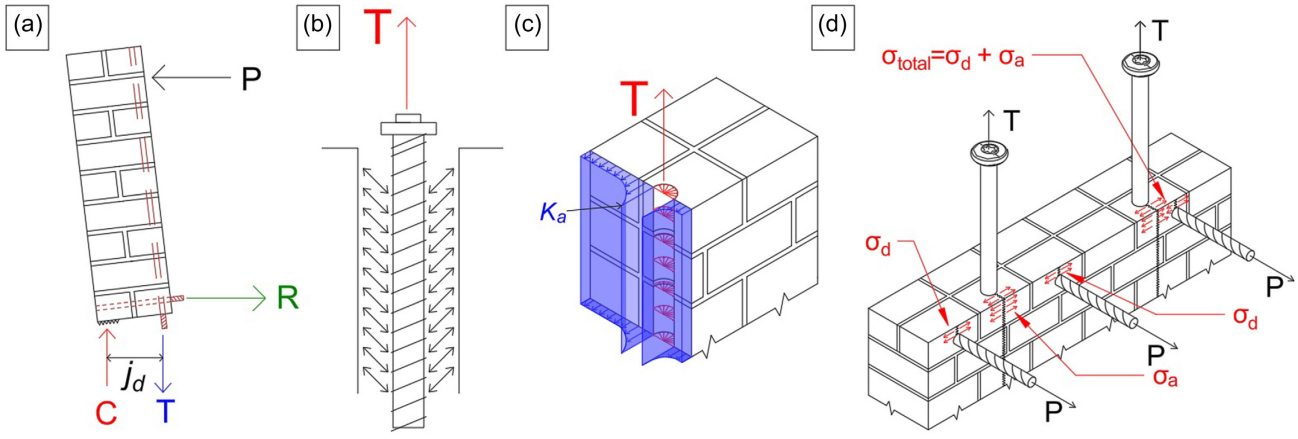


FIGURE A1 | Mechanics and assumptions behind derivation of lateral strength model.

19448201, 2026, 2, Downloaded from https://onlinelibrary.wiley.com/doi/10.1002/eqs4.70065 by University Of Auckland, Wiley Online Library on [24/06/2026]. See the Terms and Conditions (https://onlinelibrary.wiley.com/terms-and-conditions) on Wiley Online Library for rules of use; OA articles are governed by the applicable Creative Commons License

TABLE A1 | Assumptions to simplify Equation (A-6).

Approximation	Description
$l_{emb,d} \approx 0.66 t_w$	The embedment of the diaphragm anchors will extend a minimum of 2/3 into the parapet wall
$t_w - D \approx 0.8d$	The thickness of the cross section minus the anchor diameter is close to the internal lever arm as estimated by $0.8d$
$d \approx t_w$	One of the terms for d is replaced by t_w for convenience as they are close in length
$l_{emb,a} \leq 300\,\text{mm}$	Experimental data showed that there was no significant benefit in extending the anchor embedment beyond 300 mm in terms of the anchor pullout strength

$$\begin{aligned}\sigma'_x &= K_a\left(\frac{D}{t_w - D}\right)\sigma_x = K_a\left(\frac{D}{t_w - D}\right)\int_{-\frac{\pi}{2}}^{\frac{\pi}{2}} \sigma_r \cos\,\theta\, d\theta \\ \sigma_x &= K_a\left(\frac{D}{t_w - D}\right)2\sigma_r \\ \sigma'_x &= \frac{2K_a T}{\pi l_{emb}(t_w - D)}\end{aligned} \tag{A-4}$$

where the σ'_x represents the largest splitting stresses and all other terms as defined previously.

Given that there are two sources contributing to splitting tension in the brick from the vertical anchors (σ_a) and the horizontal diaphragm anchors (σ_d) as shown in Figure A1d, the two actions can be combined such that failure is defined by when their sum reaches the brick's tensile strength (f_t):

$$\begin{aligned}f_t &= \sigma_a + \sigma_d \\ f_t &= \frac{2K_a T_1}{\pi l_{emb,a}(t_w - D)} + \frac{2K_d T_2}{\pi l_{emb,d} D}\end{aligned} \tag{A-5}$$

For σ_d, the effective zone over which the splitting tensile stresses apply is taken as D instead of $(t_w - D)$ for conservatism. Substituting Equations (A-1) and (A-2), which estimate the vertical and diaphragm anchor forces, into Equation (A-5) results in a useful expression for design:

$$P = \frac{\pi f_t}{\frac{2hK_a}{l_{emb,a}(t_w - D)0.8d\left(\frac{b_w}{s_a}\right)} + \frac{2K_d}{Dl_{emb,d}\left(\frac{b_w}{s_d}\right)}} \tag{A-6}$$

A couple of simplifications were made to make Equation (A-6) easier to apply (see Table A1). With these simplifying assumptions, this results in the simplified design equations of

$$P = \frac{0.66\pi f_t}{\frac{2hK_a}{l_{emb,a} d t_w (b_w/s_a)} + \frac{2K_d}{D t_w (b_w/s_d)}} \tag{A-7}$$

Note that $\frac{0.66\pi}{2} \approx 1$. Algebraically manipulating the terms, we can arrive at the functional form:

$$P = \lambda b_w t_w f_t, \quad \lambda = \lambda = \frac{1}{\frac{hs_a}{dl_{emb,a}}K_a + \frac{s_p}{D}K_d} \tag{A-8}$$

To select the values for K_a and K_d that best fit the equation, a nonlinear minimization was used to find the minimum of the mean squared error when the nominal strength equation is compared to the experimental results. This resulted in the values of $K_a = 2.4$ and $K_b = 0.21$. For simplicity, the values of $K_a = 2$ and $K_b = 0.2$ were adopted. This is consistent with the physical problem because it is expected that most of the contribution to splitting pullout comes from the vertical anchors (larger value of K_a) and a much lesser but still noticeable effect by the diaphragm anchors (smaller value of K_b). With these selected values, the final design equations become as presented in the body of the article:

$$P_{ap} = \lambda t_w b_w f_t \tag{A-9}$$

where λ is taken as

$$\lambda = \frac{0.5}{\frac{hs_a}{dl_{emb,a}} + \frac{s_p}{10D}} \tag{A-10}$$

19448201, 2026, 2, Downloaded from https://onlinelibrary.wiley.com/doi/10.1002/eqs4.70065 by University Of Auckland, Wiley Online Library on [24/06/2026]. See the Terms and Conditions (https://onlinelibrary.wiley.com/terms-and-conditions) on Wiley Online Library for rules of use; OA articles are governed by the applicable Creative Commons License

Appendix B

Design Equation Summary and Worked Example

$$V_u \le \psi V_n$$

Probability of exceedance	ψ
20%	0.80
15%	0.75
10%	0.70
5%	0.60

$$V_n = \min\left(P_{mt}, P_{mc}, P_{ar}, P_{ap}\right)$$

P_{mt} (Flexural mortar cracking)	Calculate by suitable design code (e.g., ASCE 41 − 23)
P_{mc} (brick crushing)	$P_{mc} = \frac{0.15d^2 b_{w,eff}}{h} f_{c,min}$
	$b_{w,eff} = 300N$ mm if $s_a \ge 300$ mm
	$f_{c,min} = \min(f_c, f_{cm})$
P_{ar} (anchor rupture)	$P_{ar} = \frac{0.8A_s d}{h} f_u$
P_{ap} (anchor pullout)	$P_{ap} = \lambda t_w b_w f_t$
	$\lambda = \frac{0.5}{\frac{hs_a}{dl_{emb,a}} + \frac{s_p}{10D}}$
	$l_{emb,a} \le 300$ mm

Example:

Consider a 500-mm-tall two-wythe parapet that runs along one perimeter of a building that is 10 m in length. An anchor spacing of 500 mm is used for both vertical and diaphragm anchoring. Vertical anchors are 1.0 m in length. Determine the lateral strength by considering P_{mc}, P_{ar}, and P_{ap}. The brick and mortar have the same mean compressive strength of 10 MPa.

Solution:

Since there is not enough information about the structure to estimate P_{mt}, this step is neglected in this worked example. First, we estimate the number of anchors needed given the spacing and parapet length, and other geometric quantities:

$$\text{Number of anchors} = N_a = \frac{10{,}000 \text{ mm}}{500 \text{ mm}} = 20 \text{ anchors}$$

Since the spacing of anchors exceeds 300 mm, a reduced width in flexural compression is necessary. This is estimated as

$$b_{w,eff} = 300 \text{ mm} \times 20 = 6000 \text{ mm}$$

A two-wythe parapet wall is estimated at $t_w = 230$ mm and the anchor is installed at the centroid of the brick. Generally, we assume a distance of 50 mm from the edge of the parapet wall to the anchor

$$d = 230 - 50 = 180 \text{ mm}$$

To estimate the lateral strength associated with brick crushing:

$$P_{mc} = \frac{0.15d^2 b_{w,eff}}{h} f_{c,min} = \frac{0.15(180 \text{ mm})^2 (6000 \text{ mm})}{500 \text{ mm}} (10 \text{ MPa}) = 583 \text{ kN}$$

To estimate the lateral strength associated with anchor rupture:

$$P_{ar} = \frac{0.8A_s d}{h} f_u = \frac{0.8(50 \text{ mm}^2 \times 20 \text{ anchors})(180 \text{ mm})}{500 \text{ mm}} (1040 \text{ MPa}) = 300 \text{ kN}$$

Next, we estimate the lateral strength associated with anchor pullout. Although the embedded distance $l_{emb,a}$ is the length of the anchor minus height of the wall (i.e., 1000–500 = 500), we take $l_{emb,a} \le 300$. Plugging this in, we get

19448201, 2026, 2, Downloaded from https://onlinelibrary.wiley.com/doi/10.1002/eqs4.70065 by University Of Auckland, Wiley Online Library on [24/06/2026]. See the Terms and Conditions (https://onlinelibrary.wiley.com/terms-and-conditions) on Wiley Online Library for rules of use; OA articles are governed by the applicable Creative Commons License

$$\lambda = \frac{0.5}{\frac{hs_a}{dl_{emb,a}} + \frac{s_p}{10D}} = \frac{0.5}{\frac{(500\,\text{mm})(500\,\text{mm})}{(180\,\text{mm})(300\,\text{mm})} + \frac{300}{10(8)}} = 0.06$$

$$P_{ap} = \lambda t_w b_w f_{ct} = (0.06)(230\,\text{mm})(10,000\,\text{mm})(0.05 \times 10\,\text{MPa}) = 68.6\,\text{kN}$$

Since $P_{ap} < P_{ar} < P_{mc}$, the limiting strength is 68.8 kN. Or in terms of the base shear coefficient, using an assumed unit weight of 1600 kg/m^3, we get

$$\frac{68.8\,\text{kN}}{1600\,\frac{\text{kg}}{\text{m}^3} \times 10\,\text{m} \times 0.5\,\text{m} \times 0.23\,\text{m}} \cdot \frac{1\,\text{g}}{9.81\,\frac{\text{m}}{\text{s}}} = 3.8$$

19448201, 2026, 2, Downloaded from https://onlinelibrary.wiley.com/doi/10.1002/eqs4.70065 by University Of Auckland, Wiley Online Library on [24/06/2026]. See the Terms and Conditions (https://onlinelibrary.wiley.com/terms-and-conditions) on Wiley Online Library for rules of use; OA articles are governed by the applicable Creative Commons License